Patterns and trends of atmospheric mercury in the GMOS network: Insights based on a decade of measurements

Mariantonia Bencardino, Francesco D'amore, Hélène Angot, Lorenzo Angiuli, Yann Bertrand, Warren Cairns, María Diéguez, Aurélien Dommergue, Ralf Ebinghaus, Giulio Esposito, et al.

Environmental Pollution 363 (2024) 125104

Contents lists available at ScienceDirect

Environmental Pollution

journal homepage: www.elsevier.com/locate/envpol

Patterns and trends of atmospheric mercury in the GMOS network: Insights based on a decade of measurements☆

Mariantonia Bencardino [a,*], Francesco D'Amore [b], Hélène Angot [c], Lorenzo Angiuli [d], Yann Bertrand [c], Warren Cairns [e,f], María C. Diéguez [g], Aurélien Dommergue [c], Ralf Ebinghaus [h], Giulio Esposito [i], Kateřina Komínková [j], Casper Labuschagne [k], Valentino Mannarino [a], Lynwill Martin [k], Maria Martino [a], Luis Mendes Neves [l], Nikolay Mashyanov [m], Olivier Magand [n], Peter Nelson [o], Claus Norstrom [p], Katie Read [q], Sergey Sholupov [m], Henrik Skov [p], Antonella Tassone [a], Gabriela Vítková [j], Sergio Cinnirella [a], Francesca Sprovieri [a], Nicola Pirrone [a]

[a] CNR-Institute of Atmospheric Pollution Research, Rende, Italy
[b] CNR-Institute for High Performance Computing and Networking, Rende, Italy
[c] Univ. Grenoble Alpes, CNRS, INRAE, IRD, Grenoble INP, IGE, Grenoble, France
[d] Apulia Region Environmental Protection Agency, Bari, Italy
[e] CNR-Institute of Polar Sciences, Mestre, Italy
[f] Ca' Foscari-University of Venice, Venice, Italy
[g] INIBIOMA-CONICET-UNComa, San Carlos de Bariloche, Argentina
[h] Helmholtz-Zentrum Hereon, Institute of Coastal Environmental Chemistry, Germany
[i] CNR-Institute of Atmospheric Pollution Research, Montelibretti, Italy
[j] Global Change Research Institute of the Czech Academy of Sciences, Brno, Czech Republic
[k] South African Weather Service, South Africa
[l] Cape Verde Observatory, INMG, São Vicente, Cabo Verde
[m] Lumex-marketing LLC, St. Petersburg, Russia
[n] Observatoire des Sciences de l'Univers de La Réunion, UR, CNRS, Meteo-France, IRD, Saint-Denis, La Réunion, France
[o] Macquarie University, Sydney, Australia
[p] Department of Environmental Science, iClimate, Arctic Research Center, Aarhus University, Roskilde, Denmark
[q] National Centre for Atmospheric Science, University of York, UK

ARTICLE INFO

Dataset link: https://gos4m.org/, https://doi.org/10.25326/168, https://doi.org/10.25326/348, https://doi.org/10.25326/350, https://gmos.aeris-data.fr/

Keywords:
Atmospheric mercury
Global mercury observation system (GMOS)
Hemispheric gradient
Temporal trends
Seasonal variability

ABSTRACT

The Global Mercury Observation System (GMOS) network, initially a five-year project (2010–2015) funded by the European Commission, continued as a GEO Flagship program to support the Global Observation System for Mercury (GOS4M). GMOS was envisioned as a coordinated global observing system to monitor atmospheric mercury (Hg) on a global scale, to support and evaluate the effective implementation of the Minamata Convention on Mercury (MCM). Twenty-eight ground-based stations have participated in monitoring activities, following GMOS sampling protocols and related data quality control management. The GMOS network provides representative coverage of all latitudes, from the Northern Hemisphere to the Southern Hemisphere including the Arctic Circle, Antarctica, and the Tropical Zone. This work presents atmospheric Hg data, available as Total Gaseous Mercury (TGM) or Gaseous Elemental Mercury (GEM) concentrations, recorded within the GMOS network from 2011 to 2020. TGM/GEM concentrations were analysed in terms of their variability along latitudinal areas, considering their comparability, temporal trends and patterns. The main results confirmed a clear gradient of TGM/GEM concentrations between the northern (1.58 ± 0.31 ng/m^3) and southern (0.97 ± 0.14 ng/m^3) hemispheres. Decreasing trends in TGM/GEM levels were found to be strongly significant only for selected remote stations with at least 5 years of data coverage. Seasonality in atmospheric TGM/GEM concentrations was observed to increase with latitude and is greater at inland sites than at coastal sites.

☆ This paper has been recommended for acceptance by Michael Bank.

* Corresponding author.
E-mail address: mariantonia.bencardino@cnr.it (M. Bencardino).

https://doi.org/10.1016/j.envpol.2024.125104
Received 28 April 2024; Received in revised form 16 September 2024; Accepted 8 October 2024
Available online 28 October 2024

1. Introduction

The atmosphere is one of the key parts of the biogeochemical mercury (Hg) cycle, serving as a reactor for physicochemical interactions of Hg species, influencing transport and deposition mechanisms, and thus determining their global distribution. Hg displays complex speciation and chemistry in the atmosphere, which influences its temporal and spatial behaviour, and thereby the impact of Hg pollution on ecosystems and human health. Understanding atmospheric Hg processes at regional and global scales is therefore necessary to assess worldwide impacts of this toxic metal. Due to its volatility and the relatively long atmospheric lifetime of its elemental form, Hg can be transported on a global scale and deposited remote from emission sources, therefore it is considered a "global pollutant" (Lindberg et al., 2007; Gustin and Jaffe, 2010; Travnikov et al., 2017). During the last two decades, extensive efforts have been made to improve the understanding of spatial and temporal patterns of atmospheric Hg on a global scale (Sprovieri et al., 2016; Custodio et al., 2020). Several monitoring and modelling studies have focused on the fate and transport of Hg and have provided recommendations and future directions on the need to develop globally harmonized observing networks to better assess the global distribution of tropospheric Hg. The goal is to provide consistent, quality assured and quality controlled (QA/QC) Hg measurements, which are essential inputs for regional and global-scale models. These models can be used for the production of more accurate predictions of future Hg scenarios, which, in turn are necessary for the design of effective emission control policies. To date, all the existing atmospheric Hg monitoring networks, including the Arctic Monitoring and Assessment Program (AMAP – Dietz et al., 2022; MacSween et al., 2022), the Environment and Climate Change Canada - Atmospheric Mercury Monitoring Network (ECCC-AMM - Temme et al., 2007; Cole et al., 2014), the United States Atmospheric Mercury Network (AMNet - Gay et al., 2013), the Asia Pacific Mercury Monitoring Network (APMMN -Sheu et al., 2019), the European Monitoring and Evaluation Program (EMEP - Tørseth et al., 2012), the Global Mercury Observation System (GMOS Sprovieri et al., 2016), and the recently established South African Mercury Network (SAMNet), have a clear agreement in terms of instrumentation, measurement techniques, maintenance and standard operating procedures (SOPs) (Gay et al., 2013; Steffen et al., 2012; D'Amore et al., 2015; Sprovieri et al., 2016). The GMOS network (www.gmos.eu), was established in 2010 as an EU-funded project "Global Mercury Observation System", with the aim to integrate existing monitoring sites and establish new facilities in areas where Hg observations have been lacking (i.e., in South and Middle East Asia, and South America). The need to ensure data consistency among the operational network, led to the implementation and adoption of a centralized Data Quality Management System (G-DQM) (D'Amore et al., 2015). G-DQM is based on existing common SOPs and QA/QC protocols from both the Canadian and US networks, as well as on the European standard procedures for Hg. The GMOS network additionally complies the data sharing principles established by the Group on Earth Observations (GEO), which aims to develop a Global Earth Observation System of Systems (GEOSS) using "observation platforms". The establishment of an interoperable e-infrastructure in line with the requirements of GEO has been one of the main achievements of the GMOS network (Cinnirella et al., 2014; D'Amore et al., 2015). GMOS activities are currently part of the GEO flagship GOS4M (Global Observation System for Mercury - www.gos4m.org), which was established to support international efforts to control this persistent pollutant (Pirrone et al., 2022; De Simone et al., 2021). This also provided support for UNEP's activities under Articles 19 and 22 of the Minamata Convention on Mercury (MCM), which relate to "research, development and monitoring", and "evaluation of effectiveness", respectively. In this paper we present an updated dataset of atmospheric elemental Hg, in terms of Total Gaseous Mercury (TGM) or Gaseous Elemental Mercury (GEM) concentrations, at selected GMOS ground-based sites, distributed over the Northern and Southern Hemispheres, the Tropics and both the Polar regions. The available TGM/GEM data collected during 10 years of monitoring, over the 2010–2020 time-span, were analysed in terms of their spatio-temporal variability.

2. Materials and methods

2.1. The GMOS network

The general strategy of the GMOS project (2010–2015) was to develop and improve a state-of-the-art observation network capable of providing information on Hg concentrations in ambient air and deposition at global scale (Sprovieri et al., 2016, 2017). After 2015, the end of the related EU-funded GMOS, the GMOS network continued to operate under the GOS4M program, a GEO Flagship in support of the MCM. At this stage, a small number of monitoring sites have been relocated or closed due to the high operational costs of instrumentation and measurement management. Overall, a total of 28 stations, whose classification is summarized in Table A.1 while additional information and characteristics with respect to TGM/GEM measurements are reported in Table A.2. As pointed out within the mentioned tables, the GMOS stations were grouped based on their location and within distinct meridian bands, at different latitudes (lat): the Arctic (ARC, lat: 66.5° N - 90° N) or the Antarctic (ANC, lat: 66.5° S - 90° S), the Northern Hemisphere (NH; lat: 23.5° N - 66.5° N); the Tropical Zone (TZ, lat: 23.5° S - 23.5° N), or the Southern Hemisphere (SH, lat: 66.5° S - 90° S). It is thus evident that, even if the distribution of the number of stations in some parts is smaller, there is sufficient coverage to appreciate spatial differences in different countries of the world, as well as hemispheric variability.

2.2. GMOS sampling sites

Most of the GMOS sites (~80%) are classified as remote (14) and rural (8) stations, and many of them contribute to the Global Atmosphere Watch (GAW) program of the World Meteorological Organization (WMO) (see Table A.1). The remaining GMOS stations are suburban (3) and urban (2). Regarding the environmental characteristics of the surrounding areas, the GMOS network includes 14 sampling sites representative of coastal (marine and lacustrine) and 8 high-altitude (mountain) stations distributed over various world regions (see Fig. 1). The remaining sampling sites, 6 stations, that are neither coastal nor high altitude, are otherwise classified as continental (see Table A.1).

Within the GMOS network, monitoring sites at the highest latitudes are those located in the Arctic and the Antarctic areas: Villum Research Station (VRS), in the north-eastern corner of Greenland (Skov et al., 2020; Goodsite et al., 2004, 2012; Wang et al., 2019); Dumont d'Urville (DDU), located in a small Antarctic island (Angot et al., 2016b), and Concordia station, at Dome C (DMC) in the Antarctic plateau (Cairns et al., 2021; Song et al., 2018; Spolaor et al., 2018; Angot et al., 2016c,a). In the NH, there are 3 remote high-altitude sites in Asia: the EvK2CNR (EVK) Pyramid Observatory, in the eastern Himalaya Mountains of Nepal (Gratz et al., 2013); the Mt. Ailao (MAL) station, in a subtropical evergreen forest in southwestern China (Zhang et al., 2016b); and the Mt. Walinguan (MWA) station, at the north-eastern edge of the Tibetan Plateau (Zhang et al., 2021). There is a remote station representative of continental conditions at Mt. Changbai (MCH), in a temperate deciduous mixed forest in north-eastern China (Fu et al., 2012, 2015). The easternmost area within the NH is covered by the rural station Listvyanka (LIS), located in Siberia (Russia), at the shore of Lake Baikal (Mashyanov et al., 2021). On the European side, there are also two remote sites: the Mace Head (MHE) GAW station, on the western coast of Ireland in the North Atlantic (Custodio et al., 2020; Weigelt et al., 2015); and the Col Margherita (CMA) GAW regional station, located in the Belluno Dolomites, between the Veneto and

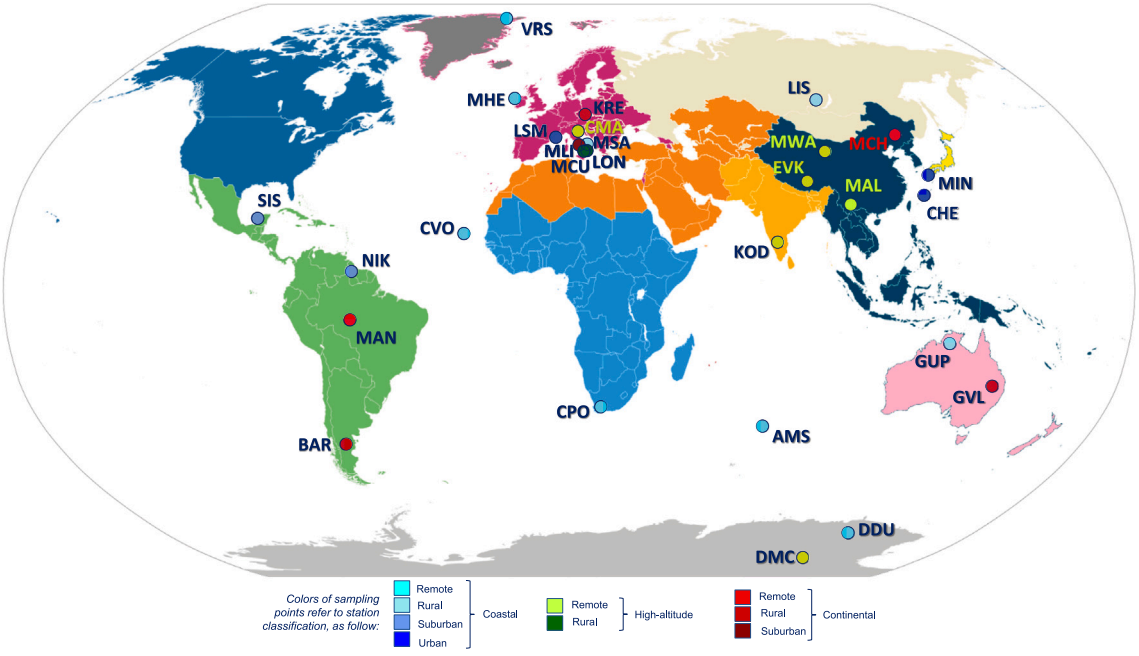

Fig. 1. Location of the GMOS network monitoring stations included in this study. Different colours used for sampling sites refer to station classification: Coastal (Remote, Rural, Suburban, and Urban), High-altitude (Remote, and Rural), and Continental (Remote, Rural, and Suburban).

Trentino-Alto Adige regions, in north-eastern Italy (Vardè et al., 2022). In Europe, there are 4 rural stations,of which 2 are located in the Sila Massif of the Southern Apennine Mountain chain in the Calabria region: the Longobucco (LON) station (D'Amore et al., 2015; Bencardino et al., 2011) then replaced in 2014 by the Monte Curcio (MCU) regional GAW station (Bencardino et al., 2019; Moretti et al., 2021; Castagna et al., 2021). Other rural stations are the Monte Sant'Angelo (MSA), located on the slopes of the Gargano ridge in the Apulia Region, facing the Adriatic Sea, (Martino et al., 2022); and the Křešín u Pacova (KRE) continental station, in central Czech Republic (Dvorská et al., 2015; Veselik et al., 2017).

Within TZ, there are 4 GMOS sites, of which 3 are remote: the continental station of Manaus (MAN), of the Brazilian Agricultural Research Corporation (De Simone et al., 2017; da Silva Palácios et al., 2020); the coastal station Calhau (CVO), located in the Cape Verde archipelago, in the central Atlantic Ocean (Read et al., 2017); and the high-altitude Kodaikanal (KOD) site, in the western side of South India (Karthik et al., 2017). The only rural site within TZ is the coastal station Gunn Point (GUP), located in the savannah of the Northern Territory of Australia (Howard et al., 2017). In the SH there are only 4 GMOS stations, of which 2 are remote coastal sites influenced by oceanic fetch of the southern ocean, in the case of the Cape Point (CPO) GAW station, in the southernmost point of Africa (Slemr et al., 2015, 2020; Martin et al., 2017); and by the Indian and Southern oceans, in the case of the isolated Amsterdam Island (AMS) global GAW station (Angot et al., 2014; Slemr et al., 2015, 2020; Magand et al., 2023; Tassone et al., 2023). The remaining 2 GMOS sites in the SH are representative of rural continental conditions: the Bariloche (BAR) station, in southern South America located in the Andean belt, inside the Nahuel Huapi National Park (NHNP) in north-western Patagonia (Argentina) (Diéguez et al., 2019, 2022); and the Glenville (GVL) station, located in the south-western part of the Australian peninsula (Morrison et al., 2015).

The GMOS network also includes 3 suburban stations, one in the NH, the Montelibretti (MLI) EMEP continental station, in central Italy (Massimi et al., 2022); and 2 coastal sites in the TZ: the Sisal (SIS) station, located in the north-western coast of Yucatán (Mexico) in Central America (Sena et al., 2015); and the Nieuw Nickerie (NIK) station,in the west coast of Suriname in north-eastern South America (Müller et al., 2012). Further, the GMOS network has 3 urban stations in the NH, two in the coast of Japan, Minamata (MIN) next to Minamata Bay (Marumoto and Imai, 2015); and Cape Hedo (CHE), in the Okinawa Island bordering the East China Sea and the Pacific Ocean (Marumoto et al., 2019); while La Seyne-sur-Mer (LSM) is in a harbour area on the south-eastern coast of France, in the Provence-Alpes-Côte d'Azur region (Marusczak et al., 2016).

2.3. Measurement methods and GMOS protocols

This study refers to atmospheric Hg monitoring, focusing mainly on measurements of Total/Elemental Gaseous Mercury species (TGM/GEM), where TGM is the sum of Reactive Gaseous Mercury (RGM) and GEM. However, since RGM is almost 3 orders of magnitude lower than TGM, its levels are assumed to not significantly affect TGM vs GEM comparisons (Duan et al., 2017). Within the GMOS network, TGM/GEM levels were mainly determined through three different approaches and detail of the specific Hg species detected, whether TGM or GEM, is reported in Table A.2, for each involved monitoring station. Hg was measured as TGM in those stations only equipped with an automated Hg vapor Tekran 2537 analyser (versions A, B or X), based on the Cold Vapour Atomic Fluorescence Spectroscopy (CVAFS) technique (TEKRAN, 1998). Otherwise, it was detected as GEM, in the case the Tekran 2537 analyzer was used together with the Tekran speciation unit (1130/1135 modules), making it possible to discriminate RGM from GEM. At some sites, GEM species was determined using the Lumex RA-915 mercury monitor, which performs a direct continuous measurement of GEM concentrations in air flow, based on differential Atomic Absorption Spectroscopy (AAS) with Zeeman effect (Sholupov et al., 2004, 2022). Despite operational differences between CVAFS and AAS techniques, comparative studies between the Tekran 2537 and RA-915, performed during the development of a

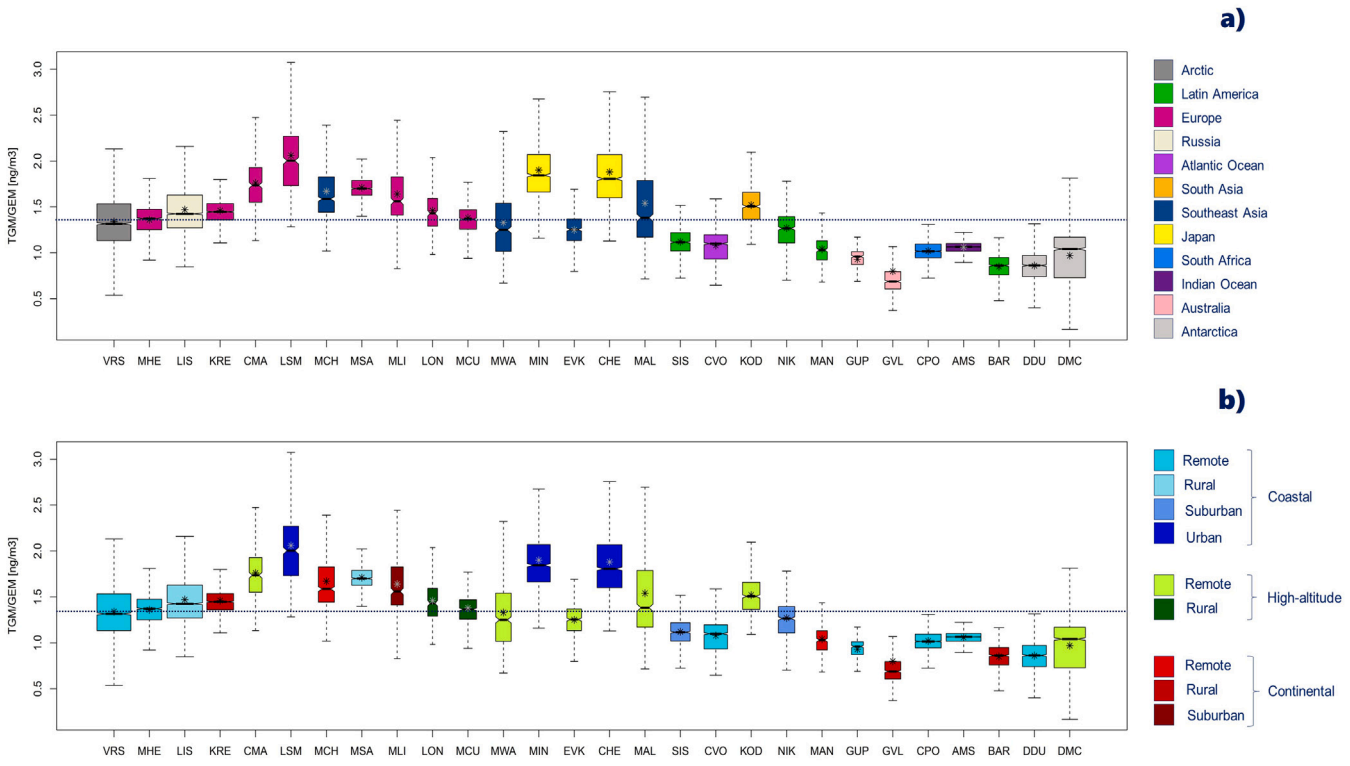

Fig. 2. Box plots (with interquartile ranges), and mean values (*) showing variability of daily TGM/GEM valid data recorded at each GMOS station, over the time-period indicated in Table A.2. Width of each box is proportional to the number of TGM/GEM valid observations recorded at the corresponding station. Used colours refer to the following categorization: (a) location; and (b) station classification. Median of all observations is reported in both graph as reference (dotted horizontal line).

standard method for the determination of ambient air quality (UNI EN 15852:2010), showed good agreement in the measurements obtained by both systems (Brown et al., 2010), also confirmed by recent work based on field intercomparisons and the propagation of errors in the concentration calculations (Brown et al., 2010; Gustin et al., 2024; Andron et al., 2024; de Krom et al., 2021; Berisha et al., 2020). In addition, Hg measurements carried out within the GMOS network followed harmonized SOPs; that have been recognized, evaluated, and adopted by the scientific community of reference, thus enabling proper comparisons between different measurement results (Munthe et al., 2011; Steffen et al., 2012).

2.4. Data management and trend-analysis methodology

Data from all sampling stations were acquired by the ad- hoc GMOS Cyber Infrastructure (Cinnirella et al., 2014), and processed, to ensure their quality assurance and quality control (QA/QC), by a web-based GMOS-Data Quality Management System (G-DQM) (D'Amore et al., 2015). The latter is a centralized platform, specifically developed to collect all the Hg raw data coming from the GMOS stations in one dedicated database. The QA process was defined in strict compliance with the GMOS SOPs and is automatically applied through the G-DQM processing chain. Site managers of each station are able to access online the G-DQM system, check results coming from the QA process, and then provide their expert supervision. Details about each component and the operation of the G-DQM system are discussed in D'Amore et al. (2015).

Validated Hg data resulting from the G-DQM application are finally archived at the dedicated GMOS repository website (http://sdi.iia.cnr.it/gmos). As the only exception, data from AMS, DMC and DDU stations were qualified following a data management system specifically developed by Magand et al. (2023). This is alternative system is in compliance with the GMOS SOPs. Hg data from AMS, DDU and DMC, once validated through this application, were both archived under the official GMOS project repository and also, under the GMOS-FR (Global Mercury Observation System - France, https://www.aeris-data.fr/projects/gmos-fr/) dedicated French database (Magand et al., 2023). Daily/monthly averages were used to provide summary statistics for each site, requiring 75% of data coverage within the hour/month of reference. The resulting quality-controlled TGM/GEM datasets, recorded over a decade (2011–2020) at the GMOS stations, are presented and discussed in the following sections. The obtained daily/monthly statistics were evaluated in terms of significant differences, firstly as a whole, using the Kruskal–Wallis test; and then for pairwise comparisons, with the Wilcoxon rank sum test, using the adjustment method of Benjamini and Hochberg (Benjamini and Yekutieli, 2001).

In order to evaluate the changes in the TGM/GEM concentrations during the period covered by this study, multi-year trend analysis has been performed using the Theil–Sen method (Theil, 1950; Sen, 1968), based on the non-parametric Mann–Kendall approach (Hirsch et al., 1982). The Mann–Kendall test can confirm or reject the presence of a trend, without providing any insight into the magnitude of the trend. This information is instead provided by the Theil–Sen method, whose advantage is that it is resistant to outliers and produces accurate confidence intervals even with non-normal data and heteroscedasticity. In line with analogous already published works (Cole and Steffen, 2010; Cole et al., 2014; Gay et al., 2013; Weiss-Penzias et al., 2016), the overall annual trends for each GMOS station, were estimated from monthly TGM/GEM concentrations, and considering a 95% confidence interval for the TheilSen slope calculations. Trend analysis was carried out only for those GMOS station having a sufficient data coverage (> 5 years of measurements), and relative outcomes presented and

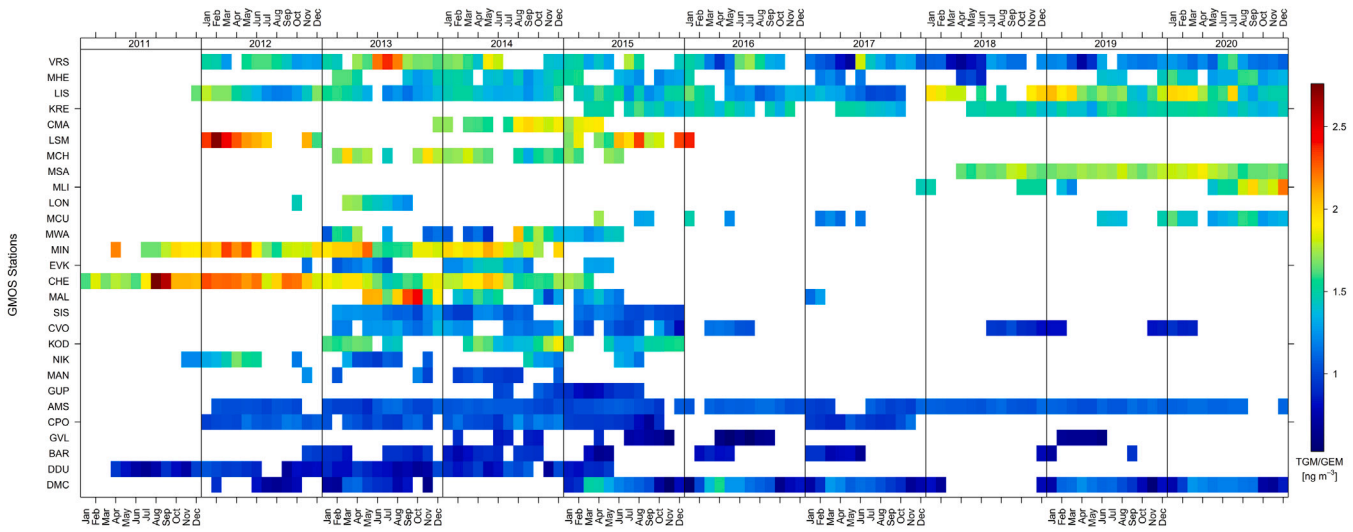

Fig. 3. Monthly averaged TGM/GEM concentrations reported for each GMOS station, over the time period 2011–2020.

discussed in terms of their statistical significance. In our work we used the Theil–Sen estimator available from the *openair* package of the free R software (Carslaw and Ropkins, 2012). By using this Theil–Sen function we derived *p* values associated with the trend slopes, so that to provide information about the statistical significance of the trend estimates. The *p* value and all uncertainties were calculated through bootstrap resampling simulations, that provides more robust estimates of these parameters. The basic function has been adapted to take account of auto-correlated data using block bootstrap simulations based on Kunsch (1989).

3. Results and discussion

3.1. TGM/GEM from a 10-year database: data consistency and spatial variability

This study focused on a ten years (2011–2020) period during which almost continuous monitoring of quality-assured TGM/GEM measurements was realized by LIS station, with 9 years data coverage achieved by VRS and AMS, and MHE, BAR and DMC, each contributing 8 years of measurements. Of a total of 28 stations involved in the GMOS network, 13 have provided valid TGM/GEM data for more than 5 years. The remaining 15 sites produced TGM/GEM data with a lower annual coverage, of between 2 and 4 years (see Table A.1).

Available valid TGM/GEM daily measurements are summarized in Table A.3 and highlighted in Fig. 2, where two different colour categorizations were used: one referring to the allocated region (Fig. 2 a), and the other to the station classification (Fig. 2 b). The median of all observations recorded at all GMOS stations was found to be equal to 1.34 ng/m^3 and it is reported in Fig. 2 for reference. As confirmed by the Kruskal–Wallis rank sum test, there were significant differences between daily measurements at the GMOS stations, whose pairwise comparisons were also carried out using the Wilcoxon rank sum test, showing strong statistical difference for most of the GMOS stations ($p < 0.001$).

The dual-colour categorization was used to provide a direct and useful visualization of the variability of the TGM/GEM concentrations observed at each GMOS monitoring site, with respect to their location and station classification. From Fig. 2(a) it can be easily observed that stations showing median values higher than the overall median (1.34 ng/m^3) are located in the NH; and specifically from measurements at the two Japanese (MIN and CHE) stations, the Indian (KOD), European (LSM, CMA, MSA, MLI), and at the majority of Chinese (MCH and MAL). It can also be recognized that the highest median TGM/GEM values are recorded at LIS (2.0 ± 0.29 ng/m^3), MIN (1.85 ± 0.34 ng/m^3) and CHE (1.81 ± 0.40 ng/m^3), all classified as urban coastal stations (see Fig. 2 (b). Independently of region, remote high-altitude stations recording higher TGM/GEM median values such as: CMA (1.74 ± 0.32 ng/m^3) in Europe, MAL (1.38 ± 0.53 ng/m^3) in China, and KOD (1.50 ± 0.19 ng/m^3) in India, are sites situated at the same elevation, around 2500 m a.s.l., whilst MWA and EVK, both at much higher altitudes, around 3800 and 5000 m a.s.l., respectively, reported significantly lower median TGM/GEM values, equal to 1.25 ± 0.42 ng/m^3, and 1.25 ± 0.18 ng/m^3, respectively (statistically insignificant each other). This has been observed previously and is possibly due to elevation specific atmospheric dynamics differently influencing the air quality at these sites (Xing and Jin, 2023; Mao et al., 2016). Another interesting result is that at the MCH Chinese station, classified as a remote continental site; the average TGM/GEM values (1.71 ± 0.20 ng/m^3), is significantly higher than those detected at the other remote/rural continental stations, such as KRE, MAN, and GVL, and is likely due to the fact that MCH station belongs to the Asia-Pacific region, whose Hg emission sources represent the major contributor to the global distribution (Brocza et al., 2024).

Monthly TGM/GEM averages were also computed for these datasets and considered representative only when available daily data covered at least 75% of the corresponding reference month. Monthly availability of TGM/GEM, thus defined, is reported in Table A.3 for each station and each year of observation, whereas the corresponding TGM/GEM values are shown in Fig. 3. These latter values provide an overview on the operational activity period of each station, also returning the spatio-temporal variability of TGM/GEM levels detected, from 2011 to 2020, within the whole GMOS network. It can be observed from this figure the averaged monthly TGM/GEM levels above 2 ng/m^3 (shown in orange, red and brown in Fig. 3), are mainly detected in stations of the NH, while values below 1 ng/m^3 (marked in blue in Fig. 3), are mainly recorded at stations covering the SH and the ANC.

3.2. TGM/GEM inter- and intra-hemispheric gradient

In order to understand drivers and mechanisms involved in the atmospheric Hg cycle on a global scale, and to assess the inter-hemispheric

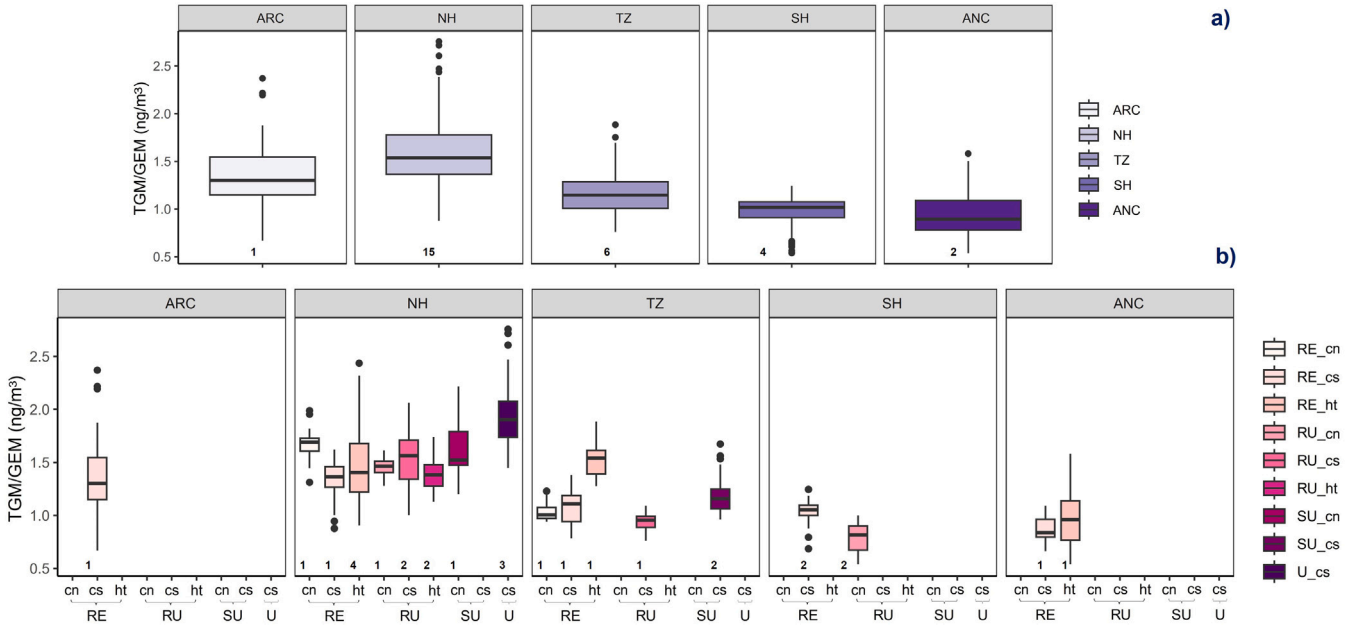

Fig. 4. Box and whisker plots of monthly TGM/GEM concentrations, with respect to: (a) inter-hemispheric gradient considering the Arctic Circle (ARC), Northern Hemisphere (NH), Tropical Zone (TZ), Southern Hemisphere (SH), and Antarctic Circle (ANC); (b) intra-hemispheric gradient within each identified geographic latitudinal area, and between different station classification: remote continental (RE-cn), remote coastal (RE-cs), remote high-altitude (RE-ht), rural continental (RU-cn), rural coastal (RU-cs), rural high-altitude (RU-ht), suburban continental (SU-cn), suburban coastal (SU-cs), and urban coastal (U-cs).

gradient, the available TGM/GEM data from the 28 GMOS stations were re-arranged into subsets, corresponding to each of the five related geographic zones (ARC, NH, TZ, SH, ANC). Therefore, TGM/GEM levels in the NH were evaluated considering the complete datasets from the 15 stations within this geographic zone (namely, MHE, LIS, KRE, CMA, LSM, MCH, MSA, MLI, LON, MCU, MWA, MIN, EVK, CHE, and MAL). In addition, TGM/GEM levels in TZ and SH included the full datasets from 6 (SIS, CVO, KOD, NIK, MAN, and GUP) and 4 (AMS, CPO, GVL, and BAR) sampling sites, respectively. For both remote polar regions, only a few stations were included, namely: VRS, the unique GMOS station representative for ARC, and DDU and DMC stations, for ANC. The variability of the recorded monthly TGM/GEM concentrations were found to be statistically different between each of the considered 5 geographic bands (Wilcoxon test, p-values < 0.001), and their distributions are shown in the box-and-whisker plot in Fig. 4.a).

These findings, in line to those similarly alluded to by Sprovieri et al. (2016), could be affected by the limited GMOS stations in the SH and along the TZ. Important contributors to atmospheric Hg emissions in the tropical SH regions are those relating to the use of mercury in artisanal and small-scale gold mining (ASGM), in addition to emissions from natural sources such as wildfires (Fisher et al., 2023), and a thorough evaluation of these is not possible considering the GMOS stations in this study. However, the inter-hemispherical TGM/GEM gradient herein exploiting the large amount of data in the GMOS database, complements and is in-line with findings reported elsewhere, including those based either on lake sediment and peat records of Hg deposition, and on those using global modelling analysis (Li et al., 2020; Horowitz et al., 2017).

Overall, the GMOS network datasets, showed TGM/GEM concentrations higher in the NH (1.58 ± 0.31 ng/m^3), decreasing gradually towards the TZ (1.17 ± 0.23 ng/m^3) and the SH (0.97 ± 0.14 ng/m^3), and displaying the lowest concentration at ANC (0.93 ± 0.21 ng/m^3). Measurements from stations in the TZ; such as Maido Observatory, in Reunion Island in the middle of Indian ocean, and the high altitude Chacaltaya station in Bolivia; not included in the GMOS network, showed mean TGM/GEM concentrations comparable with those reported in this study (Koenig et al., 2021, 2023). TGM/GEM mean levels observed at the VRS station, herein considered representative for the ARC region (1.35 ± 0.32 ng/m^3), were found to be in the middle of the range of value recorded within the NH and TZ regions; and almost 30% higher than those detected in this study for ANC. As reported by MacSween et al. (2022), TGM levels observed at VRS station were lower in comparison with those recorded in further high-Arctic coastal sites, such as Alert and Zeppelin. Although the ARC is a remote region, with limited contamination from local anthropogenic Hg sources, it is influenced by long-range transport of Hg-contaminated air masses that, due to global circulation, are able to affect the North Pole from NH mid-latitudes (Skov et al., 2020).

To investigate the overall variability detected within each of the 5 identified geographic bands, an additional analysis, considering station classification, was further carried out. The GMOS network includes 9 different categories associated with station classification, namely: remote continental (RE-cn), remote coastal (RE-cs), remote high-altitude (RE-ht), rural continental (RU-cn), rural coastal (RU-cs), rural high-altitude (RU-ht), suburban continental (SU-cn), suburban coastal (SU-cs), and urban coastal (U-cs). TGM/GEM datasets corresponding to each of these categories, were considered as further subsets within each latitudinal band. The resulting distribution for each TGM/GEM subset is shown as a box-plot in Fig. 4(b), and the number of stations included within the analysis for each box is also indicated. This figure shows that the patterns emerging from station classification, were not consistent in all the geographical areas. In fact, within the NH the highest statistically significant TGM/GEM mean value (1.92 ± 0.26 ng/m^3, $p<0.001$) is recorded at monitoring sites classified as urban coastal stations and the lowest TGM/GEM levels were captured by both remote coastal, remote high-altitude, and rural high-altitude stations, with mean values, statistically similar to each-other ($p>0.1$), equal to 1.35 ± 0.16 ng/m^3, 1.46 ± 0.33 ng/m^3, and 1.39 ± 0.16 ng/m^3,

respectively. This is a similar finding to observations in the US (AMNet sites) by Angot et al. (2021), who reported levels of ~ 1.7 ng/m^3 for urban sites, and values of ~ 1.4 ng/m^3 for rural sites. However, within the TZ region, the highest statistically significant (p<0.001) TGM/GEM levels were from measurements made in the high-altitude remote station category, with a mean TGM/GEM concentration equal to 1.52 ± 0.15 ng/m^3, and were 41% and 46% higher than those recorded at both coastal (1.08 ± 0.16 ng/m^3), and continental (1.04 ± 0.09 ng/m^3) remote stations, respectively. The value recorded for the high-altitude category within the TZ area was additionally found to be significantly greater than the corresponding TGM/GEM value recorded not only at rural coastal station (0.93 ± 0.10 ng/m^3), but also at those monitoring sites representative of the suburban continental category (1.18 ± 0.16 ng/m^3), in contrast to the findings from the NH data here and the previous US study. This outcome can be in part explained by the fact that, within the TZ region, the high-altitude remote category is represented by KOD station, located in India, where local activities, among which it is noteworthy to mention agricultural residue burning, represent important sources of Hg emissions (Sahu et al., 2024).

The extensive observations described here, although in general confirm the inter-hemispheric gradient, further indicate that within each geographical band, the main intra-hemispheric differences between TGM/GEM concentrations cannot be exclusively explained by the classification of monitoring stations. An understanding of the site specific seasonal and monthly variability of Hg and the effect on atmospheric dynamics is needed as this can greatly influence the Hg budget in terms of TGM/GEM concentrations.

3.3. TGM/GEM site-specific seasonal and monthly patterns

For datasets covering the whole period investigated in this study (2011–2020), daily TGM/GEM levels, differentiated by latitudinal coverage and by station classification, were considered in Fig. A.6. The figure highlights the larger variability detected at both urban/suburban and remote stations in the NH. Comparable TGM/GEM levels were recorded in urban stations at the European (LSM) and Japanese (CHE and MIN) stations and the suburban MLI station, consistent with its classification, reported lower TGM/GEM than these. In contrast, the remote stations within the NH, showed a clear differentiation between the only coastal station MHE, and those located at high-altitude. In fact, measurements at remote high-altitude stations, such as at the Chinese MAL and MWA, and the Italian CMA, the daily TGM/GEM levels reached maximum values well above 3 ng/m^3, while MHE reported values ranging between 1 and 2 ng/m^3. A similar difference was observed in the TZ region, between the remote high-altitude KOD station KOD, that showed higher values and wider variability compared to the coastal CVO station. Various behaviours were also detected in terms of monthly patterns Fig. A.7.

A total of 8 stations within the NH, most of them in Europe, showed higher TGM/GEM values (1.52 – 2.29 ng/m^3) in winter, from January to March, associated with emissions from the increased heating demand (Weigelt et al., 2015) and lower TGM/GEM concentrations were recorded during summer, from July to September, coinciding with elevated TGM/GEM oxidation rates during warmer months (Horowitz et al., 2017; Martino et al., 2022). These patterns agree with those reported in Custódio et al. (2021). In addition, the TGM/GEM monthly patterns observed in the NH could also be influenced by the enhanced vegetation uptake during the growing season which removes TGM/GEM from the air and incorporates it into the standing crop (Jiskra et al., 2019; Obrist et al., 2017). Moreover, a higher seasonal variation in atmospheric TGM/GEM concentrations is observed in data obtained at inland, and high-altitude sites, compared to from coastal ones, that could additionally in part be explained by the effect of the vegetation uptake (Jiskra et al., 2018).

Considering the data from the remote stations within the NH region, see Fig. A.7(c), the monthly variability is high when the higher TGM/GEM concentrations (> 1.50 ng/m^3) are recorded, between August and October. These correspond to two of the high-altitude Chinese stations (MAL and MWA), and is likely related with the influence of monsoonal climate in southwestern China during this period of the year (Zhang et al., 2016a). Contrasting with stations of the NH, those from the SH showed lower variability in the monthly TGM/GEM, but consistent with records discussed elsewhere by Slemr et al. (2020) and Zimmermann et al. (1989). This is also explained by the Hg uptake of terrestrial vegetation that, due to land distribution, is smaller in the SH (Jiskra et al., 2018). Monthly averaged TGM/GEM concentrations for ARC and ANC were plotted separately, to better highlight their unusual characteristics Fig. A.8.

In ARC, the lowest mean TGM/GEM concentration (1.10 ± 0.54 ng/m^3) was recorded in April, and increased afterwards by about a third in July (1.68 ± 0.41 ng/m^3). This pattern has been linked to atmospheric mercury depletion events (AMDEs), a typical phenomena of the polar areas during spring, followed by Hg re-emission from ice/snow in the polar summer (Skov et al., 2004; Steffen et al., 2008; Cole and Steffen, 2010; Angot et al., 2016b; Skov et al., 2020; Araujo et al., 2022; Yue et al., 2023). In late summer the GEM concentrations detected at VRS, started decreasing and by fall they then reached the average background levels (~ 1.24 ng/m^3), similar to what has been observed elsewhere at Zeppelin station, Ny-Alesund, Svalbard, in the Arctic environment (Berg et al. 2013; Angot, 2016c) (Angot et al., 2016a).

Regarding the ANC area, slight monthly changes were recorded at the DDU station (min= 0.73 ± 0.05 ng/m^3, Max= 0.96 ± 0.10 ng/m^3), whereas at the high-altitude DMC station, in the Antarctic Plateau, the maximum concentration (1.31 ± 0.18 ng/m^3) was observed during the austral spring while the minimum (0.62 ± 0.10 ng/m^3) observed in summer, consistent with previous studies describing the seasonal variation of TGM/GEM concentrations at Antarctic sites (Angot et al., 2016b).

3.4. Long-term trends for selected monitoring stations

Following the trend-analysis methodology described in the dedicated paragraph, TGM/GEM long-term trends were computed only for stations with available data coverage over at least 5 years. Results were expressed in terms of the slopes of the trends themselves, and expressed as the change in the averaged concentration/year (in our case, ng/m^3/yr), and additionally, as the percentage change (%/year).

As summarized in Table A.4, our estimates showed highly significant trends (p < 0.001 or p < 0.01) at only 8 GMOS monitoring sites, whose monthly averaged TGM/GEM time series, together with the estimated Theil–Sen's slope and associated uncertainties, are shown in Fig. 5.

Negative trends were detected for VRS, in the ARC region, over the 2012–2020 time-span, with a negative rate of change equal to −0.060 ng/m^3/yr, comparable to that reported in MacSween et al. (2022), where a data coverage from 2008 to 2018 is considered. Negative trends for VRS herein presented are found to be more pronounced in respect to that reported in Skov et al. (2020), where trend analysis was carried out over a larger historical dataset (1999–2017 but including a data gap from 2003 to 2008). This outcome for the VRS station would seem to confirm that declines of TGM/GEM concentrations in Arctic have accelerated over the last decade (MacSween et al., 2022; Zhang et al., 2016b). The general declining TGM/GEM trends observed in our study for stations such as MHE, LIS, and CHE, within the NH region, is in agreement with the decreasing atmospheric Hg levels reported in previous studies (Zhang et al., 2016b), and is likely associated with a general anthropogenic emission reduction (Zhang et al., 2023). For MHE and LIS sites, both coastal monitoring stations, located in Europe and in Russia, respectively, significant down-ward trends were detected over shorter subsetted period in the available data. For MHE we found a significant negative trend (−0.098 ng/m^3/yr, p< 0.01) over

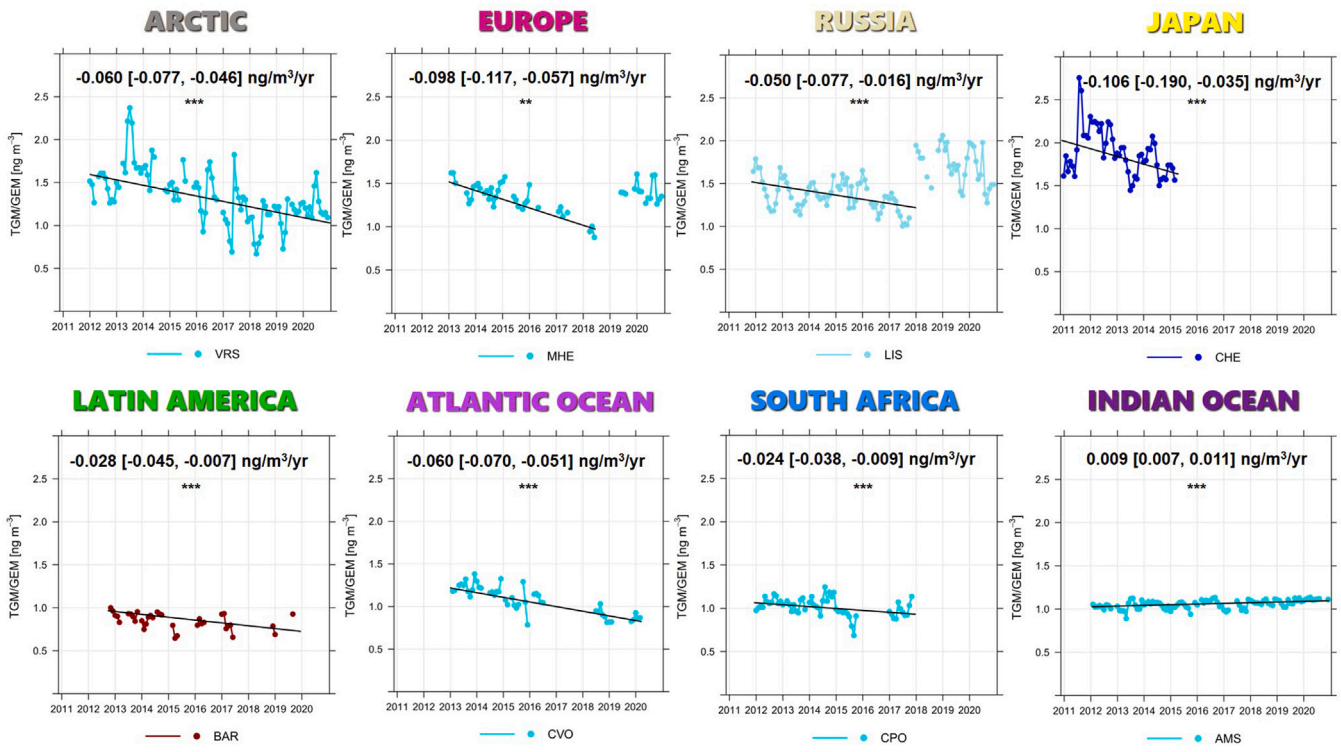

Fig. 5. Trend analysis results for GMOS stations with data coverage over more than five years. Theil–Sen's slope and uncertainties estimates are also reported with their statistical significance (p<0.001=*** and p<0.01=**).

the period 2013–2018, while for LIS, the estimated strongly significant trend (−0.050 ng/m^3/yr, p< 0.001) was observed over the 2012–2018 time-span. These patterns could be partially affected by the contrasting emissions trends observed in recent years, which are declining in Europe, specifically as EU28, and increasing in eastern Asia and the Commonwealth of Independent States (CIS) (AMAP and UNEP, 2019).

A decline rate equal to −0.060 ng/m^3/yr was also observed at CVO station, in the middle of the Atlantic Ocean, results in line with the previous estimates made by Read et al. (2017). This negative trend is also in agreement with the output of the GEOS-CHEM analysis for the northern Atlantic and attributed to changing in Hg concentrations in subsurface seawater (Soerensen et al., 2012). For the SH, statistically significant descending annual slopes were found for both the CPO station and BAR stations. An estimate of −0.024 ng/m^3/yr was detected for the CPO stations, thus confirming the slight downward trend starting in 2012 as also detected in other studies (Slemr et al., 2020; Bieser et al., 2020). A similar long-term trend slope value, equal to −0.028 ng/m^3/yr, was also estimated for the BAR station. The monitoring area surrounding this station in Patagonia is characterized by specific geomorphological conditions, such as the presence of volcanoes along the Andes Mountains, as well as air masses coming from the Atlantic Ocean, which deserve further investigation with respect to their influence on the observed trend of atmospheric mercury (Diéguez et al., 2019; Schneider et al., 2023).

Our analysis suggested an exception in the data from AMS station, in the Indian Ocean, that showed a tiny but strongly significant increasing trend of about 0.009 ng/m^3/yr, over the observed time period (2012–2020). This could be related with re-emission from the ocean, whose influence could be an important factor (Bieser et al., 2020; Zhang et al., 2023). Both stations in the ANC region (DDU and DMC), with more than five years of data coverage, did not show any significant trends. Changes in Hg concentration trends certainly reflect changes in source/sink emissions but climate and other environmental factors play a key role that, as provided by modelled scenarios, would have even more emphasis in the next decades (Dastoor et al., 2022; Slemr et al., 2011; Streets et al., 2019; Zhang et al., 2023).

4. Conclusions and future remarks

This overview summarized the spatio-temporal variations of TGM/GEM in various world regions with different local environmental characterization, and also considering the latitudinal gradient. The updated TGM/GEM database, available for selected GMOS stations, and presented for the first time as a whole in this work, will contribute to the overall goal of further comprehension about Hg cycling on a global scale. The study on TGM/GEM levels, resulting from atmospheric monitoring activities carried out between 2011 and 2020, within the GMOS network, made it possible to observe a clear inter-hemispheric differentiation for which substantial new information on intra-hemispheric variability has been gained. Despite the lack of monitoring stations in the equatorial and southern hemisphere compared to those available within the northern band, those sites were however well placed to offer insight into the influences important for these regions. The highest levels of TGM/GEM were observed in the Northern Hemisphere compared to all other regions at lower latitudes ranging from the Tropical Zone to the Southern Hemisphere, and also higher than the levels measure in both polar areas. The resulting TGM/GEM behaviour was largely influenced by the surrounding conditions of the specific geographical areas, in which data were collected. Higher concentrations, and also a larger variability in TGM/GEM levels was found to be more associated with stations at high-altitude and, primarily those located in continental Asian.

Long-term TGM/GEM measurements at coastal-specific sites indicated an overall declining trend. Limited measurements in Antarctica suggest not significant trends while within the Indian Ocean a slight increasing trend was detected, probably affected by re-emission from the ocean. The re-emissions from ocean and also from land are estimated to contribute even more to the Hg emission budget in the future decades due to climate change and this requires deeper understanding. The Minamata Convention effectiveness evaluation will largely depend on the magnitude of the re-emissions, and that requires a comprehensive understanding of the global Hg cycle. A reliable assessment on the mechanisms affecting the observed trends already represents a complex challenge, and it would substantially benefit from integration with modelling analysis and updated emission inventories, for each region of the world. It is certainly imperative to integrate modelling and measuring outcomes but also the monitoring of long-term trends in TGM/GEM needs to continue, ideally increasing the number and the distribution of monitoring station in some key areas of the world such as in the TZ, SH and polar regions.

CRediT authorship contribution statement

Mariantonia Bencardino: Writing – original draft, Validation, Methodology, Investigation, Formal analysis, Data curation, Conceptualization. **Francesco D'Amore:** Validation, Software, Methodology, Data curation. **Hélène Angot:** Writing – review & editing, Validation, Formal analysis, Data curation. **Lorenzo Angiuli:** Data curation. **Yann Bertrand:** Data curation. **Warren Cairns:** Data curation. **María C. Diéguez:** Writing – review & editing, Formal analysis, Data curation. **Aurélien Dommergue:** Writing – review & editing, Validation, Formal analysis, Data curation. **Ralf Ebinghaus:** Data curation. **Giulio Esposito:** Validation, Data curation. **Kateřina Komínková:** Data curation. **Casper Labuschagne:** Writing – review & editing, Data curation. **Valentino Mannarino:** Data curation. **Lynwill Martin:** Writing – review & editing, Data curation. **Maria Martino:** Data curation. **Luis Mendes Neves:** Data curation. **Nikolay Mashyanov:** Data curation. **Olivier Magand:** Writing – review & editing, Validation, Formal analysis, Data curation. **Peter Nelson:** Data curation. **Claus Norstrom:** Data curation. **Katie Read:** Writing – review & editing, Data curation. **Sergey Sholupov:** Data curation. **Henrik Skov:** Data curation. **Antonella Tassone:** Data curation. **Gabriela Vítková:** Data curation. **Sergio Cinnirella:** Supervision, Data curation. **Francesca Sprovieri:** Writing – review & editing, Supervision, Conceptualization. **Nicola Pirrone:** Supervision, Funding acquisition.

Funding support

The Authors would like to acknowledge the contribution received from the following ongoing project:

- FET Proactive project "Towards new frontiers for distributed environmental monitoring based on an ecosystem of plant seed-like soft robots" (I-Seed), funded by the EU's Horizon 2020 research and innovation programme under grant agreement No 101017940;
- EIRENE PPP funded by the EU's HORIZON EUROPE - HORIZON-INFRA-2021-DEV-02, Grant Agreement No. 101079789.

Finally, the authors acknowledge the support received from the past projects:

- Global Mercury Observation System - GMOS funded by the European Commission within the FP7 (GA N-265113);
- Amsterdam Island, Dome Concordia and Dumont D'Urville atmospheric mercury data, accessible in GMOS-FR national database (https://gmos.aeris-data.fr/) have been collected with funding from European Union 7th Framework Programme project Global Mercury Observation System (GMOS 2010–2015), the French Polar Institute (IPEV) via GMOStral-1028 IPEV program since 2012, the LEFE CHAT CNRS/INSU the Institut Universitaire de France and the H2020 ERA-PLANET (689443) iGOSP programme;
- AU received financial support from the Danish Environmental Protection Agency for continuous funding over the years from the "Danish Program for Arctic Research".

Declaration of competing interest

The authors declare that they have no known competing financial interests or personal relationships that could have appeared to influence the work reported in this paper.

Acknowledgements

The Authors would like to acknowledge all the institutional partners and their representatives and also staff members who have contributed to design and develop the GMOS network. A special mention of acknowledgement for the following research teams/institutes/agencies:

- All the overwintering staff at AMS, DMC, DDU and the French Polar Institute Paul-Emile Victor (IPEV) and TAAF staff and scientists who helped with the setup and maintenance of the experiment at these sites in the framework of the GMOStral-1028 IPEV program. AMS, DMC and DDU GEM data were collected via instruments coordinated by the IGE-PTICHA technical platform dedicated to atmospheric chemistry field instrumentation as well as also from CNR-IIA instruments for DMC site. The authors acknowledge the AERIS data infrastructure for providing access to the atmospheric mercury data in this study;
- The Natural Environmental Research Council (NERC) and the Atmospheric Measurement and Observation Facility (AMOF), National Centre for Atmospheric Science (NCAS) for their sustained funding of the Cape Verde Observatory;
- The Ministry of Education, Youth and Sports of CR within the CzeCOS program, grant number LM2023048;
- The Royal Danish Air Force is acknowledged by AU for providing free transport of the equipment to Villum Research Station, and the staff at Station Nord are especially acknowledged for their excellent technical support;
- The Limnological Institute of the Siberian Branch of the Russian Academy of Sciences (LIN SB RAS), for supporting the long-term mercury monitoring at the LIS station.

Appendix. Supplementary material

See Tables A.1–A.4 and Figs. A.6–A.8.

Data availability

Data are available as follow:

• GMOS database is available on request at https://gos4m.org/;
• AMS levels 1 and 2 GEM data (https://doi.org/10.25326/168 for L2), DMC levels 1 and 2 GEM data (https://doi.org/10.25326/348 for L2) and DDU level 1 GEM data (https://doi.org/10.25326/350) are also freely available at https://gmos.aeris-data.fr/ from GMOS-FR AERIS data portal coordinated by IGE (Institut des Géosciences de l'Environnement, Grenoble, France) with the support of the French national AERIS-SEDOO partners, data and services center for the atmosphere (last access: 04 April 2023).

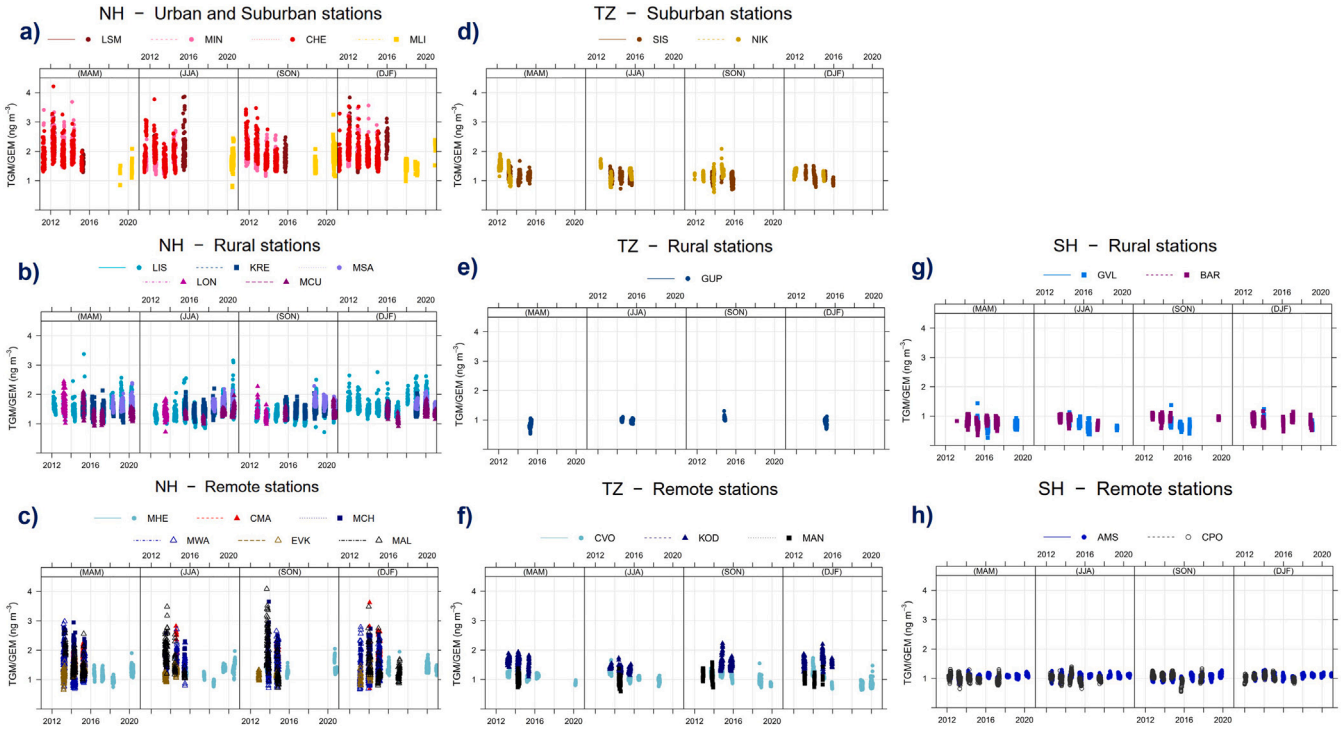

Fig. A.6. Daily TGM/GEM variability, by seasons and by station classification, in NH (a), (b), (c), TZ (d), (e), (f), and SH (g) and (h).

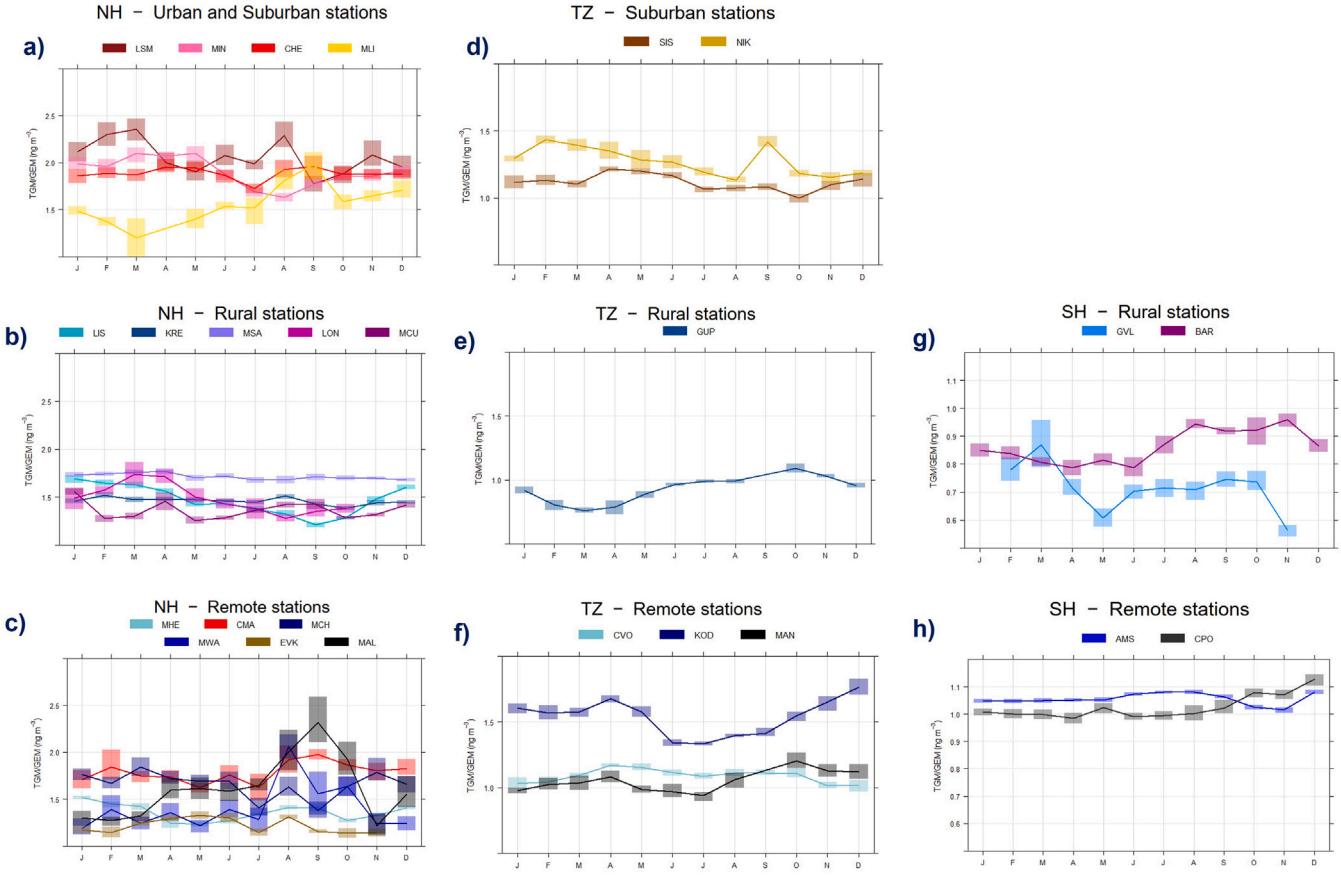

Fig. A.7. Monthly TGM/GEM variability, by station classification, in NH (a), (b), (c), TZ (d), (e), (f), and SH (g) and (h).

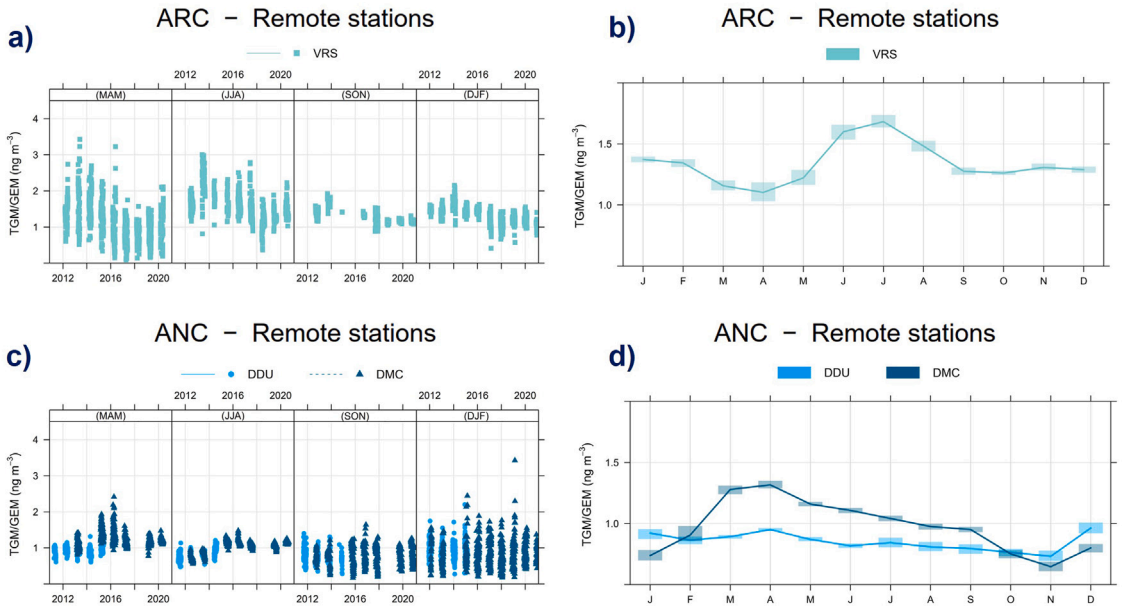

Fig. A.8. Daily/Monthly TGM/GEM variability, differentiated by seasons and station classification, at stations located in: (a)–(b), ARC and (c)–(d) ANC.

Table A.1
Ground-based monitoring sites included in the GMOS network organized by latitude. Station classification and belonging world's region are reported.

Latitudinal region	Station name	Station code	Country	Station classification
ARC	Villum Research Station	VRS	Arctic	Remote Coastal
NH	Mace Head	MHE	Europe	Remote[a] Coastal
	Listvyanka	LIS	Russia	Rural Coastal
	Kresin u Pacova	KRE	Europe	Rural Continental
	Col Margherita	CMA	Europe	Remote[b] High-altitude
	La Seyne-sur-Mer	LSM	Europe	Urban Coastal
	Mt. Changbai	MCH	Southeast Asia	Remote Continental
	Monte Sant'Angelo	MSA	Europe	Rural Coastal
	Montelibretti	MLI	Europe	Suburban Continental
	Longobucco	LON	Europe	Rural High-altitude
	Monte Curcio	MCU	Europe	Rural[b] High-altitude
	Mt. Waliguan	MWA	Southeast Asia	Remote[a] High-altitude
	Minamata	MIN	Japan	Urban Coastal
	Ev-K2	EVK	Southeast Asia	Remote[a] High-altitude
	Cape Hedo	CHE	Japan	Urban Coastal
	Mt. Ailao	MAL	Southeast Asia	Remote High-altitude
NH	Sisal	SIS	Latin America	Suburban Coastal
	Calhau	CVO	Atlantic Ocean	Remote[a] Coastal
	Kodaikanal	KOD	South Asia	Remote High-altitude
	Nieuw Nickerie	NIK	Latin America	Suburban Coastal
	Manaus	MAN	Latin America	Remote Continental
	Gunn Point	GUP	Australia	Rural[b] Coastal
SH	Amsterdam Island	AMS	Indian Ocean	Remote[a] Coastal
	Cape Point	CPO	South Africa	Remote[a] Coastal
	Glenville	GVL	Australia	Rural Continental
	Bariloche	BAR	Latin America	Rural Continental
ANC	Dumont d'Urville	DDU	Antarctica	Remote[a] Coastal
	Dome C	DMC	Antarctica	Remote[b] High-altitude

[a] Global WMO-GAW station.
[b] Regional WMO-GAW station.

Table A.2
Basic information about the GMOS monitoring station locations, the involved participating organizations, and the period of sampling considered in this study.

Station	Elevation	Lat	Lon	Participating organization	Time sampling	Hg Species
Villum Research Station	25	81,58	−16,61	AU	2012–2020	TGM
Mace Head	8	53,33	−9,90	HZG	2013–2020	TGM
Listvyanka	670	51,85	104,89	SPBSU	2011–2020	GEM
Kresin u Pacova	774	49,58	15,08	GCRI	2015–2020	GEM
Col Margherita	2545	46,37	11,79	UNIVE	2014–2015	TGM
La Seyne-sur-Mer	10	43,11	5,88	IFREMER	2012, 2015–2016	TGM
Mt. Changbai	741	42,40	128,11	IGCAS	2013–2015	GEM/TGM
Monte Sant'Angelo	125	41,66	15,94	ARPA Puglia	2018–2020	GEM/TGM
Montelibretti	48	48,10	12,63	CNR-IIA	2017–2020	GEM
Longobucco	1379	39,39	16,61	CNR-IIA	2012–2013	GEM
Monte Curcio	1796	39,31	16,42	CNR-IIA	2015–2020	GEM
Mt. Waliguan	3816	36,29	100,90	IGCAS	2013–2015	GEM
Minamata	20	32,23	130,40	NIMD	2011–2014	GEM
Ev-K2	5050	27,96	86,81	CNR-IIA	2012–2015	TGM
Cape Hedo	60	26,86	128,25	NIMD	2011–2015	TGM
Mt. Ailao	2503	24,54	101,03	IGCAS	2013–2015, 2017	TGM/GEM
Sisal	7	21,16	−90,05	JRC/UNAM	2013–2015	TGM
Calhau	10	16,86	−24,87	UoY	2013–2016, 2018–2020	TGM
Kodaikanal	2333	10,23	77,46	AU IOM	2013–2015	GEM
Nieuw Nickerie	1	5,96	−57,04	INTEC	2011–2015	GEM
Manaus	110	−2,89	−59,97	APLBA	2012–2014	GEM
Gunn Point	6	−12,25	131,04	MU	2014–2015	TGM
Amsterdam Island	70	−37,80	77,55	UGA-IGE	2014–2016, 2019	GEM
Cape Point	230	−34,35	18,49	SAWS	2012–2015, 2017	TGM
Glenville	85	−32,48	151,10	MU	2012–2020	GEM
Bariloche	801	−41,13	−71,42	CONICET	2013–2019	GEM
Dumont d'Urville	40	−66,66	140,00	UGA-IGE	2011–2015	GEM
Dome C	3220	−75,10	123,35	UGA-IGE CNR-IIA	2012–2013,2015/2020	GEM

Table A.3
For each year of the referenced time-span period (2011–2020), Data Coverage refers to the number of months with at least 75% of valid TGM/GEM data coverage. Number of valid daily TGM/GEM measurements (N_{days}), corresponding daily mean ± Standard Deviation (SD), and daily median, are also reported.

Station Code	Monthly data coverage										N_{days}	TGM/GEM daily mean ± SD	TGM/GEM daily median
	2011	2012	2013	2014	2015	2016	2017	2018	2019	2020			
VRS		11	11	7	7	10	12	11	11	12	2778	1.34 ± 0.41	1.32
MHE			9	11	8	2	4	3	4	11	1455	1.36 ± 0.19	1.37
LIS	1	12	11	12	11	11	10	7	12	12	2979	1.47 ± 0.29	1.43
KRE					9	10	7	8	12	12	1673	1.46 ± 0.15	1.45
CMA				9	4						423	1.77 ± 0.32	1.74
LSM		9			2	1					590	2.07 ± 0.44	2.00
MCH			8	10	4						684	1.68 ± 0.36	1.59
MSA								9	12	12	1209	1.71 ± 0.13	1.70
MLI							1	3	1	8	362	1.62 ± 0.33	1.56
LON		1	7								281	1.46 ± 0.26	1.43
MCU					3	2	4		4	11	1079	1.36 ± 0.17	1.37
MWA			7	7	6						598	1.33 ± 0.42	1.25
MIN	6	12	12	11							1263	1.89 ± 0.35	1.85
EVK		1	5	9	3						555	1.24 ± 0.18	1.25
CHE	12	12	12	12	3						1437	1.88 ± 0.40	1.81
MAL			8	8	5		2				650	1.55 ± 0.53	1.38
SIS			11	8	11						882	1.12 ± 0.15	1.12
CVO			10	7	9	5		6	4	3	1308	1.08 ± 0.18	1.10
KOD			7	10	9						713	1.52 ± 0.19	1.51
NIK	1	7	6	4	3						693	1.27 ± 0.22	1.27
MAN		1	2	6							322	1.05 ± 0.16	1.03
GUP				4	8						331	0.93 ± 0.11	0.96
AMS		9	12	12	11	11	9	12	12	9	2882	1.06 ± 0.07	1.06
CPO		12	10	12	11		11				1567	1.02 ± 0.12	1.01
GVL				5	6	6			5		623	0.72 ± 0.17	0.69
BAR		2	7	8	3	4	6	1	2		991	0.85 ± 0.13	0.86
DDU	9	10	12	10	5						1355	0.86 ± 0.19	0.86
DMC		6	10		12	12	12	3	12	12	2337	0.96 ± 0.32	1.04

Table A.4
Multi-years trend estimates through the Theil–Sen method for stations with data coverage larger than 5 years. Slope and Slope Uncertainties (95% CI) are reported as average change (ng/m^3) per year, and as percentage (%) change per year. Statistical significance of each result is also reported as follow: p < 0.001 = ***; p < 0.01 = **; p < 0.05 = *; p < 0.1 = +, and p > 0.1 (not significant) = –).

Station code	Period estimated trends	Slope (ng/m^3/yr)	Slope Uncertainties (ng/m^3/yr)	Slope (%)	Slope Uncertainties (%)	Statistical Significance
VRS	2012–2020	−0.060	[−0.077, −0.046]	−3.8	[−4.5, −3.0]	***
MHE	2013–2019	−0.098	[−0.117, −0.057]	−6.5	[−7.30, −4.05]	***
LIS	2012–2018	−0.050	[−0.077, −0.016]	−3.4	[−4.83, −1.15]	**
CHE	2011–2015	−0.160	[−0.190, −0.035]	−5.1	[−8.77, −1.82]	***
CVO	2013–2016; 2018–2020	−0.060	[−0.070, −0.051]	−4.8	[−5.37, −4.16]	***
AMS	2012–2020	0.009	[0.007, 0.011]	0.9	[0.63, 1.14]	***
CPO	2012–2015; 2017	−0.024	[−0.038, −0.009]	−2.2	[−3.51, −0.84]	***
BAR	2013–2019	−0.028	[−0.045, −0.007]	−3.0	[−4.76, −0.85]	***
DDU	2011–2015					–
DMC	2012–2013; 2015–2020					–

References

AMAP, UNEP, 2019. Technical Background Report for the Global Mercury Assessment 2018. Arctic Monitoring and Assessment Programme (AMAP).

Andron, T.D., Corns, W.T., Živković, I., Ali, S.W., Vijayakumaran Nair, S., Horvat, M., 2024. A traceable and continuous flow calibration method for gaseous elemental mercury at low ambient concentrations. Atmos. Meas. Tech. 17 (4), 1217–1228.

Angot, H., Barret, M., Magand, O., Ramonet, M., Dommergue, A., 2014. A 2-year record of atmospheric mercury species at a background Southern Hemisphere station on Amsterdam Island. Atmos. Chem. Phys. 14, 11461–11473. http://dx.doi.org/10.5194/acp-14-11461-2014.

Angot, H., Dastoor, A., De Simone, F., Gårdfeldt, K., Gencarelli, C.N., Hedgecock, I.M., Langer, S., Magand, O., Mastromonaco, M.N., Nordstrøm, C., et al., 2016a. Chemical cycling and deposition of atmospheric mercury in polar regions: review of recent measurements and comparison with models. Atmos. Chem. Phys. 16 (16), 10735–10763.

Angot, H., Dion, I., Vogel, N., Legrand, M., Magand, O., Dommergue, A., 2016b. Multi-year record of atmospheric mercury at Dumont d'Urville, East Antarctic coast: continental outflow and oceanic influences. Atmos. Chem. Phys. 16 (13), 8265–8279.

Angot, H., Magand, O., Helmig, D., Ricaud, P., Quennehen, B., Gallée, H., Del Guasta, M., Sprovieri, F., Pirrone, N., Savarino, J., et al., 2016c. New insights into the atmospheric mercury cycling in central Antarctica and implications on a continental scale. Atmos. Chem. Phys. 16 (13), 8249–8264.

Angot, H., Rutkowski, E., Sargent, M., Wofsy, S.C., Hutyra, L.R., Howard, D., Obrist, D., Selin, N.E., 2021. Atmospheric mercury sources in a coastal-urban environment: a case study in Boston, Massachusetts, USA. Environ. Sci. Process. Impacts 23 (12), 1914–1929.

Araujo, B.F., Osterwalder, S., Szponar, N., Lee, D., Petrova, M.V., Pernov, J.B., Ahmed, S., Heimbürger-Boavida, L.E., Laffont, L., Teisserenc, R., et al., 2022. Mercury isotope evidence for Arctic summertime re-emission of mercury from the cryosphere. Nature Commun. 13 (1), 4956.

Bencardino, M., Andreoli, V., D'Amore, F., De Simone, F., Mannarino, V., Castagna, J., Moretti, S., Naccarato, A., Sprovieri, F., Pirrone, N., 2019. Carbonaceous aerosols collected at the observatory of Monte Curcio in the Southern Mediterranean Basin. Atmosphere 10 (10), 592.

Bencardino, M., Sprovieri, F., Cofone, F., Pirrone, N., 2011. Variability of atmospheric aerosol and ozone concentrations at marine, urban, and high-altitude monitoring stations in southern Italy during the 2007 summer Saharan dust outbreaks and wildfire episodes. J. Air Waste Manage. Assoc. 61 (9), 952–967.

Benjamini, Y., Yekutieli, D., 2001. The control of the false discovery rate in multiple testing under dependency. Ann. Statist. 1165–1188.

Berisha, S., Živković, I., Kotnik, J., Mlakar, T.L., Horvat, M., 2020. Quantification of total mercury in samples from cement production processing with thermal decomposition coupled with AAS. Accreditat. Qual. Assur. 25, 233–242.

Bieser, J., Angot, H., Slemr, F., Martin, L., 2020. Atmospheric mercury in the southern hemisphere–Part 2: source apportionment analysis at Cape point station, South Africa. Atmos. Chem. Phys. 20 (17), 10427–10439.

Brocza, F.M., Rafaj, P., Sander, R., Wagner, F., Jones, J.M., 2024. Global scenarios of anthropogenic mercury emissions. EGUsphere 2024, 1–33.

Brown, R., Pirrone, N., van Hoek, C., Horvat, M., Kotnik, J., Wangberg, I., Corns, W., Bieber, E., Sprovieri, F., 2010. Standardization of a European measurement method for the determination of total gaseous mercury: results of the field trial campaign and determination of a measurement uncertainty and working range. Accred. Qual. Assur. http://dx.doi.org/10.1007/s00769-010-0636-2.

Cairns, W.R., Turetta, C., Maffezzoli, N., Magand, O., Araujo, B.F., Angot, H., Segato, D., Cristofanelli, P., Sprovieri, F., Scarchilli, C., et al., 2021. Mercury in precipitated and surface snow at Dome C and a first estimate of mercury depositional fluxes during the Austral summer on the high Antarctic plateau. Atmos. Environ. 262, 118634.

Carslaw, D.C., Ropkins, K., 2012. Openair—an R package for air quality data analysis. Environ. Model. Softw. 27, 52–61.

Castagna, J., Senatore, A., Bencardino, M., D'Amore, F., Sprovieri, F., Pirrone, N., Mendicino, G., 2021. Multiscale assessment of the impact on air quality of an intense wildfire season in southern Italy. Sci. Total Environ. 761, 143271.

Cinnirella, S., D'Amore, F., Bencardino, M., Sprovieri, F., Pirrone, N., 2014. The GMOS cyber(e)-infrastructure: advanced services for supporting science and policy. Environ. Sci. Pollut. Res. 21 (6), 4193–4208. http://dx.doi.org/10.1007/s11356-013-2308-3.

Cole, A., Steffen, A., 2010. Trends in long-term gaseous mercury observations in the Arctic and effects of temperature and other atmospheric conditions. Atmos. Chem. Phys. 10 (10), 4661–4672.

Cole, A.S., Steffen, A., Eckley, C.S., Narayan, J., Pilote, M., Tordon, R., Graydon, J.A., St. Louis, V.L., Xu, X., Branfireun, B.A., 2014. A survey of mercury in air and precipitation across Canada: patterns and trends. Atmosphere 5 (3), 635–668.

Custodio, D., Ebinghaus, R., Spain, T.G., Bieser, J., 2020. Source apportionment of atmospheric mercury in the remote marine atmosphere: Mace Head GAW station, Irish western coast. Atmos. Chem. Phys. 20 (13), 7929–7939.

Custódio, D., Slemr, F., Pfaffhuber, K.A., Spain, T.G., Pankratov, F.F., Strigunova, I., Molepo, K., Skov, H., Bieser, J., Ebinghaus, R., 2021. Odds and ends of atmospheric mercury in Europe and over northern Atlantic Ocean: Temporal trends of 25 years of measurements. Atmos. Chem. Phys. Discuss. 2021, 1–20.

da Silva Palácios, R., Romera, K.S., Curado, L.F.A., Banga, N.M., Rothmund, L.D., da Silva Sallo, F., Morais, D., Santos, A.C.A., Moraes, T.J., Morais, F.G., et al., 2020. Long term analysis of optical and radiative properties of aerosols in the Amazon Basin. Aerosol Air Qual. Res. 20 (1), 139–154.

D'Amore, F., Bencardino, M., Cinnirella, S., Sprovieri, F., Pirrone, N., 2015. Data quality through a web-based QA/QC system: implementation for atmospheric mercury data from the Global Mercury Observation System. Environ. Sci. Process. Impacts 17 (8), 1482–1492. http://dx.doi.org/10.1039/C5EM00205B.

Dastoor, A., Wilson, S.J., Travnikov, O., Ryjkov, A., Angot, H., Christensen, J.H., Steenhuisen, F., Muntean, M., 2022. Arctic atmospheric mercury: Sources and changes. Sci. Total Environ. 839, 156213.

de Krom, I., Bavius, W., Ziel, R., Efremov, E., van Meer, D., van Otterloo, P., van Andel, I., van Osselen, D., Heemskerk, M., van der Veen, A.M., et al., 2021. Primary mercury gas standard for the calibration of mercury measurements. Measurement 169, 108351.

De Simone, F., Artaxo, P., Bencardino, M., Cinnirella, S., Carbone, F., d'Amore, F., Dommergue, A., Feng, X.B., Gencarelli, C.N., Hedgecock, I.M., et al., 2017. Particulate-phase mercury emissions from biomass burning and impact on resulting deposition: a modelling assessment. Atmos. Chem. Phys. 17 (3), 1881–1899.

De Simone, F., D'Amore, F., Bencardino, M., Carbone, F., Hedgecock, I.M., Sprovieri, F., Cinnirella, S., Pirrone, N., 2021. The GOS4M knowledge hub: A web-based effectiveness evaluation platform in support of the Minamata Convention on Mercury. Environ. Sci. Policy 124, 235–246.

Diéguez, M.d.C., Arcagni, M., Rizzo, A., Pérez Catán, S., Soto Cárdenas, C., Horvat, M., Ribeiro Guevara, S., 2022. Mercury in aquatic systems of North Patagonia (Argentina): Sources, processes, and trophic transfer. Freshw. Wetl. Patagonia Ecosyst. Socioecological Aspects 163–194.

Diéguez, M.C., Bencardino, M., García, P.E., D'Amore, F., Castagna, J., De Simone, F., Cárdenas, C.S., Guevara, S.R., Pirrone, N., Sprovieri, F., 2019. A multi-year record of atmospheric mercury species at a background mountain station in Andean Patagonia (Argentina): Temporal trends and meteorological influence. Atmos. Environ. 214, 116819.

Dietz, R., Wilson, S., Loseto, L.L., Dommergue, A., Xie, Z., Sonne, C., Chételat, J., 2022. Special issue on the AMAP 2021 assessment of mercury in the Arctic. Sci. Total Environ. 843, 157020. http://dx.doi.org/10.1016/j.scitotenv.2022.157020, URL: https://www.sciencedirect.com/science/article/pii/S0048969722041171.

Duan, L., Wang, X., Wang, D., Duan, Y., Cheng, N., Xiu, G., 2017. Atmospheric mercury speciation in Shanghai, China. Sci. Total Environ. 578, 460–468.

Dvorská, A., Sedlák, P., Schwarz, J., Fusek, M., Hanuš, V., Vodička, P., Trusina, J., 2015. Atmospheric station Křešín u Pacova, Czech Republic–a Central European research infrastructure for studying greenhouse gases, aerosols and air quality. Adv. Sci. Res. 12 (1), 79–83.

Fisher, J.A., Schneider, L., Fostier, A.H., Guerrero, S., Guimarães, J.R.D., Labuschagne, C., Leaner, J.J., Martin, L.G., Mason, R.P., Somerset, V., et al., 2023. A synthesis of mercury research in the Southern Hemisphere, part 2: Anthropogenic perturbations. Ambio 52 (5), 918–937.

Fu, X., Feng, X., Liang, P., amd H Zhang, D., Ji, J., Liu, P., 2012. Temporal trend and sources of speciated atmospheric mercury at Waliguan GAW station, Northwestern China. Atmos. Chem. Phys. 12 (4), 1951–1964.

Fu, X., Zhang, H., Yu, B., Wang, X., Lin, C., Feng, X., 2015. Observations of atmospheric mercury in China: a critical review. Atmos. Chem. Phys. 15 (16), 9455–9476. http://dx.doi.org/10.5194/acp-15-9455-2015.

Gay, D., Schmeltz, D., Prestbo, E., Olson, M., Sharac, T., Tordon, R., 2013. The atmospheric mercury network: measurement and initial examination of an ongoing atmospheric mercury record across North America. Atmos. Chem. Phys. 13 (4), 10521–10546.

Goodsite, M.E., Plane, J., Skov, H., 2004. A theoretical study of the oxidation of Hg0 to HgBr2 in the troposphere. Environ. Sci. Technol. 38 (6), 1772–1776.

Goodsite, M., Plane, J., Skov, H., 2012. Correction to a theoretical study of the oxidation of Hg0 to HgBr2 in the troposphere. Environ. Sci. Technol. 46 (9), 5262. http://dx.doi.org/10.1021/es301201c.

Gratz, L., Esposito, G., Dalla Torre, S., Cofone, F., Pirrone, N., Sprovieri, F., 2013. First measurements of ambient Total Gaseous Mercury (TGM) at the EvK2CNR pyramid observatory in Nepal. In: E3S Web of Conferences. vol. 1, EDP Sciences, p. 27004.

Gustin, M.S., Dunham-Cheatham, S.M., Lyman, S., Horvat, M., Gay, D.A., Gačnik, J., Gratz, L., Kempkes, G., Khalizov, A., Lin, C.-J., et al., 2024. Measurement of atmospheric mercury: Current limitations and suggestions for paths forward. Environ. Sci. Technol. 58 (29), 12853–12864.

Gustin, M., Jaffe, D., 2010. Reducing the uncertainty in measurement and understanding of mercury in the atmosphere. Environ. Sci. Technol. 44 (7), 2222–2227, https://doi.org/10.1021/es902736k. PMID: 20184358.

Hirsch, R.M., Slack, J.R., Smith, R.A., 1982. Techniques of trend analysis for monthly water quality data. Water Resour. Res. 18 (1), 107–121.

Horowitz, H.M., Jacob, D.J., Zhang, Y., Dibble, T.S., Slemr, F., Amos, H.M., Schmidt, J.A., Corbitt, E.S., Marais, E.A., Sunderland, E.M., 2017. A new mechanism for atmospheric mercury redox chemistry: implications for the global mercury budget. Atmos. Chem. Phys. 17 (10), 6353–6371.

Howard, D., Nelson, P.F., Edwards, G.C., Morrison, A.L., Fisher, J.A., Ward, J., Harnwell, J., Van Der Schoot, M., Atkinson, B., Chambers, S.D., et al., 2017. Atmospheric mercury in the Southern Hemisphere tropics: seasonal and diurnal variations and influence of inter-hemispheric transport. Atmos. Chem. Phys. 17 (18), 11623–11636.

Jiskra, M., Sonke, J.E., Agnan, Y., Helmig, D., Obrist, D., 2019. Insights from mercury stable isotopes on terrestrial–atmosphere exchange of Hg (0) in the Arctic tundra. Biogeosciences 16 (20), 4051–4064.

Jiskra, M., Sonke, J.E., Obrist, D., Bieser, J., Ebinghaus, R., Myhre, C.L., Pfaffhuber, K.A., Wängberg, I., Kyllönen, K., Worthy, D., et al., 2018. A vegetation control on seasonal variations in global atmospheric mercury concentrations. Nat. Geosci. 11 (4), 244–250.

Karthik, R., Paneerselvam, A., Ganguly, D., Hariharan, G., Srinivasalu, S., Purvaja, R., Ramesh, R., 2017. Temporal variability of atmospheric total gaseous mercury and its correlation with meteorological parameters at a high-altitude station of the South India. Atmospheric Pollut. Res. 8 (1), 164–173.

Koenig, A.M., Magand, O., Laj, P., Andrade, M., Moreno, I., Velarde, F., Salvatierra, G., Gutierrez, R., Blacutt, L., Aliaga, D., et al., 2021. Seasonal patterns of atmospheric mercury in tropical South America as inferred by a continuous total gaseous mercury record at Chacaltaya station (5240 m) in Bolivia. Atmos. Chem. Phys. 21 (5), 3447–3472.

Koenig, A.M., Magand, O., Verreyken, B., Brioude, J., Amelynck, C., Schoon, N., Colomb, A., Ferreira Araujo, B., Ramonet, M., Sha, M.K., et al., 2023. Mercury in the free troposphere and bidirectional atmosphere–vegetation exchanges–insights from Maïdo mountain observatory in the Southern Hemisphere tropics. Atmos. Chem. Phys. 23 (2), 1309–1328.

Kunsch, H.R., 1989. The jackknife and the bootstrap for general stationary observations. Ann. Statist. 1217–1241.

Li, C., Sonke, J.E., Le Roux, G., Piotrowska, N., Van der Putten, N., Roberts, S.J., Daley, T., Rice, E., Gehrels, R., Enrico, M., et al., 2020. Unequal anthropogenic enrichment of mercury in Earth's northern and southern hemispheres. ACS Earth Space Chem. 4 (11), 2073–2081.

Lindberg, S., Bullock, R., Ebinghaus, R., Engstrom, D., Feng, X., Fitzgerald, W., Pirrone, N., Prestbo, E., Seigneur, C., 2007. A synthesis of progress and uncertainties in attributing the sources of mercury in deposition. AMBIO A J. Hum. Environ. 36 (1), 19–33.

MacSween, K., Stupple, G., Aas, W., Kyllönen, K., Pfaffhuber, K.A., Skov, H., Steffen, A., Berg, T., Mastromonaco, M.N., 2022. Updated trends for atmospheric mercury in the Arctic: 1995–2018. Sci. Total Environ. 837, 155802.

Magand, O., Angot, H., Bertrand, Y., Sonke, J.E., Laffont, L., Duperray, S., Collignon, L., Boulanger, D., Dommergue, A., 2023. Over a decade of atmospheric mercury monitoring at Amsterdam Island in the French Southern and Antarctic Lands. Sci. Data 10 (1), 836.

Mao, H., Cheng, I., Zhang, L., 2016. Current understanding of the driving mechanisms for spatiotemporal variations of atmospheric speciated mercury: a review. Atmos. Chem. Phys. 16 (20), 12897–12924.

Martin, L.G., Labuschagne, C., Brunke, E.G., Weigelt, A., Ebinghaus, R., Slemr, F., 2017. Trend of atmospheric mercury concentrations at Cape Point for 1995–2004 and since 2007. Atmos. Chem. Phys. 17 (3), 2393–2399.

Martino, M., Tassone, A., Angiuli, L., Naccarato, A., Dambruoso, P.R., Mazzone, F., Trizio, L., Leonardi, C., Petracchini, F., Sprovieri, F., et al., 2022. First atmospheric mercury measurements at a coastal site in the Apulia region: seasonal variability and source analysis. Environ. Sci. Pollut. Res. 29 (45), 68460–68475.

Marumoto, K., Imai, S., 2015. Determination of dissolved gaseous mercury in seawater of Minamata Bay and estimation for mercury exchange across air–sea interface. Mar. Chem. 168, 9–17.

Marumoto, K., Suzuki, N., Shibata, Y., Takeuchi, A., Takami, A., Fukuzaki, N., Kawamoto, K., Mizohata, A., Kato, S., Yamamoto, T., et al., 2019. Long-term observation of atmospheric speciated mercury during 2007–2018 at Cape Hedo, Okinawa, Japan. Atmosphere 10 (7), 362.

Marusczak, N., Castelle, S., de Vogüé, B., Knoery, J., Cossa, D., 2016. Seasonal variations of total gaseous mercury at a French coastal Mediterranean site. Aerosol Air Qual. Res. 16 (1), 46–60.

Mashyanov, N., Obolkin, V., Pogarev, S., Ryzhov, V., Sholupov, S., Potemkin, V., Molozhnikova, E., Khodzher, T., 2021. Air mercury monitoring at the Baikal area. Atmosphere 12 (7), 807.

Massimi, L., Pietrodangelo, A., Frezzini, M.A., Ristorini, M., De Francesco, N., Sargolini, T., Amoroso, A., Di Giosa, A., Canepari, S., Perrino, C., 2022. Effects of COVID-19 lockdown on PM10 composition and sources in the Rome Area (Italy) by elements' chemical fractionation-based source apportionment. Atmos. Res. 266, 105970.

Moretti, S., Tassone, A., Andreoli, V., Carbone, F., Pirrone, N., Sprovieri, F., Naccarato, A., 2021. Analytical study on the primary and secondary organic carbon and elemental carbon in the particulate matter at the high-altitude Monte Curcio GAW station, Italy. Environ. Sci. Pollut. Res. 28 (42), 60221–60234.

Morrison, A., Nelson, P., Howard, D., 2015. Ambient atmospheric mercury in the Hunter Valley, NSW. In: 22nd International Clean Air and Environment Conference. Melbourne, Australia, pp. 20–23.

Müller, D., Wip, D., Warneke, T., Holmes, C., Dastoor, A., Notholt, J., 2012. Sources of atmospheric mercury in the tropics: continuous observations at a coastal site in Suriname. Atmos. Chem. Phys. 12 (16), 7391–7397.

Munthe, J., Sprovieri, F., Horvat, M., Ebinghaus, R., 2011. SOPs and QA/QC Protocols Regarding Measurements of TGM, GEM, RGM, TPM and Mercury in Precipitation in Cooperation with WP3, WP4 and WP5. GMOS deliverable 6.1, CNR-IIA, IVL.

Obrist, D., Agnan, Y., Jiskra, M., Olson, C.L., Colegrove, D.P., Hueber, J., Moore, C.W., Sonke, J.E., Helmig, D., 2017. Tundra uptake of atmospheric elemental mercury drives Arctic mercury pollution. Nature 547 (7662), 201–204.

Pirrone, N., Cinnirella, S., Sprovieri, F., Hedgecock, I.M., D'Amore, F., Bencardino, M., De Simone, F., 2022. The global observation system for mercury (GOS 4 M) earth observation applications for the minamata convention on mercury. Earth Obs. Appl. Glob. Policy Framew. 177–186.

Read, K.A., Neves, L.M., Carpenter, L.J., Lewis, A.C., Fleming, Z.L., Kentisbeer, J., 2017. Four years (2011–2015) of total gaseous mercury measurements from the Cape Verde Atmospheric Observatory. Atmos. Chem. Phys. 17 (8), 5393–5406.

Sahu, S.K., Mishra, M., Mishra, A., Mangaraj, P., Beig, G., 2024. Quantification and assessment of hazardous mercury emission from industrial process and other unattended sectors in India: A step towards mitigation. J. Hazard. Mater. 470, 134103.

Schneider, L., Fisher, J.A., Diéguez, M.C., Fostier, A.H., Guimaraes, J.R., Leaner, J.J., Mason, R., 2023. A synthesis of mercury research in the Southern Hemisphere, part 1: Natural processes. Ambio 52 (5), 897–917.

Sen, P.K., 1968. Estimates of the regression coefficient based on Kendall's tau. J. Am. Statist. Assoc. 63 (324), 1379–1389.

Sena, F., Umlauf, G., Ruiz, A.A., Islas, M.R., Trejo, J.A.V., Cabrera, F.A., Vargas, I.O., 2015. Wet Deposition and Atmospheric Mercury Monitoring in Sisal, Yucatán, México, as Part of the Global Mercury Observation System (GMOS). Technical Report, JRC - EUROPEAN COMMISION, http://dx.doi.org/10.2788/823558.

Sheu, G.R., Gay, D.A., Schmeltz, D., Olson, M., Chang, S.C., Lin, D.W., Nguyen, L.S.P., 2019. A new monitoring effort for Asia: the Asia Pacific mercury monitoring network (APMMN). Atmosphere 10 (9), 481.

Sholupov, S., Pogarev, S., Ryzhov, V., Mashyanov, N., Stroganov, A., 2004. Zeeman atomic absorption spectrometer RA-915+ for direct determination of mercury in air and complex matrix samples. Fuel Process. Technol. 85 (6–7), 473–485. http://dx.doi.org/10.1016/j.fuproc.2003.11.003.

Sholupov, S., Ryzhov, V., Pogarev, S., Mashyanov, N., 2022. Automatic monitors for direct continuous mercury measurement in ambient air, hydrocarbon, and industrial gases. Limnol. Freshw. Biol. 1349–1351.

Skov, H., Christensen, J.H., Goodsite, M.E., Heidam, N.Z., Jensen, B., Wåhlin, P., Geernaert, G., 2004. Fate of elemental mercury in the Arctic during atmospheric mercury depletion episodes and the load of atmospheric mercury to the Arctic. Environ. Sci. Technol. 38 (8), 2373–2382.

Skov, H., Hjorth, J., Nordstrøm, C., Jensen, B., Christoffersen, C., Bech Poulsen, M., Baldtzer Liisberg, J., Beddows, D., Dall'Osto, M., Christensen, J.H., 2020. Variability in gaseous elemental mercury at Villum Research Station, Station Nord, in North Greenland from 1999 to 2017. Atmos. Chem. Phys. 20 (21), 13253–13265.

Slemr, F., Angot, H., Dommergue, A., Magand, O., Barret, M., Weigelt, A., Ebinghaus, R., Brunke, R., Pfaffhuber, K., Edwards, G., abd J. Powell, D.H., Keywood, M., Wang, F., 2015. Comparison of mercury concentrations measured at several sites in the Southern Hemisphere. Atmos. Chem. Phys. 15, 3125–3133. http://dx.doi.org/10.5194/acp-15-3125-2015.

Slemr, F., Brunke, E.-G., Ebinghaus, R., Kuss, J., 2011. Worldwide trend of atmospheric mercury since 1995. Atmos. Chem. Phys. 11 (10), 4779–4787.

Slemr, F., Martin, L., Labuschagne, C., Mkololo, T., Angot, H., Magand, O., Dommergue, A., Garat, P., Ramonet, M., Bieser, J., 2020. Atmospheric mercury in the Southern Hemisphere–part 1: Trend and inter-annual variations in atmospheric mercury at Cape Point, South Africa, in 2007–2017, and on Amsterdam Island in 2012–2017. Atmos. Chem. Phys. 20 (13), 7683–7692.

Soerensen, A.L., Jacob, D.J., Streets, D.G., Witt, M.L., Ebinghaus, R., Mason, R.P., Andersson, M., Sunderland, E.M., 2012. Multi-decadal decline of mercury in the North Atlantic atmosphere explained by changing subsurface seawater concentrations. Geophys. Res. Lett. 39 (21).

Song, S., Angot, H., Selin, N.E., Gallée, H., Sprovieri, F., Pirrone, N., Helmig, D., Savarino, J., Magand, O., Dommergue, A., 2018. Understanding mercury oxidation and air–snow exchange on the East Antarctic Plateau: a modeling study. Atmos. Chem. Phys. 18 (21), 15825–15840.

Spolaor, A., Angot, H., Roman, M., Dommergue, A., Scarchilli, C., Vardè, M., Del Guasta, M., Pedeli, X., Varin, C., Sprovieri, F., et al., 2018. Feedback mechanisms between snow and atmospheric mercury: Results and observations from field campaigns on the Antarctic plateau. Chemosphere 197, 306–317.

Sprovieri, F., Pirrone, N., Bencardino, M., d'Amore, F., Angot, H., Barbante, C., Brunke, E.G., Arcega-Cabrera, F., Cairns, W., Comero, S., et al., 2017. Five-year records of mercury wet deposition flux at GMOS sites in the Northern and Southern hemispheres. Atmos. Chem. Phys. 17 (4), 2689–2708.

Sprovieri, F., Pirrone, N., Bencardino, M., D'Amore, F., Carbone, F., Cinnirella, S., Mannarino, V., Landis, M., Ebinghaus, R., Weigelt, A., Brunke, E.-G., Labuschagne, C., Martin, L., Munthe, J., Wängberg, I., Artaxo, P., Morais, F., Barbosa, H.D.M.J., Brito, J., Cairns, W., Barbante, C., Diéguez, M.D.C., Garcia, P.E., Dommergue, A., Angot, H., Magand, O., Skov, H., Horvat, M., Kotnik, J., Read, K.A., Neves, L.M., Gawlik, B.M., Sena, F., Mashyanov, N., Obolkin, V., Wip, D., Feng, X.B., Zhang, H., Fu, X., Ramachandran, R., Cossa, D., Knoery, J., Marusczak, N., Nerentorp, M., Norstrom, C., 2016. Atmospheric mercury concentrations observed at ground-based monitoring sites globally distributed in the framework of the GMOS network. Atmos. Chem. Phys. 16 (18), 11915–11935. http://dx.doi.org/10.5194/acp-16-11915-2016, URL: http://www.atmos-chem-phys.net/16/11915/2016/.

Steffen, A., Douglas, T., Amyot, M., Ariya, P., Aspmo, K., Berg, T., Bottenheim, J., Brooks, S., Cobbett, F., Dastoor, A., Dommergue, A., Ebinghaus, R., Ferrari, C., Gardfeldt, K., Goodsite, M., Lean, D., Poulain, A., Scherz, C., Skov, H., Sommar, J., Temme, C., 2008. A synthesis of atmospheric mercury depletion event chemistry in the atmosphere and snow. Atmos. Chem. Phys. 8, 1445–1482. http://dx.doi.org/10.5194/acp-8-1445-2008.

Steffen, A., Scherz, T., Olson, M., Gay, D., Blanchard, P., 2012. A comparison of data quality control protocols for atmospheric mercury speciation measurements. JEM 14 (3), 752–765.

Streets, D.G., Horowitz, H.M., Lu, Z., Levin, L., Thackray, C.P., Sunderland, E.M., 2019. Global and regional trends in mercury emissions and concentrations, 2010–2015. Atmos. Environ. 201, 417–427.

Tassone, A., Magand, O., Naccarato, A., Martino, M., Amico, D., Sprovieri, F., Leuridan, H., Bertrand, Y., Ramonet, M., Pirrone, N., et al., 2023. Seven-year monitoring of mercury in wet precipitation and atmosphere at the Amsterdam Island GMOS station. Heliyon 9 (3).

TEKRAN, 1998. Model 2357A principles of operation. Tekran Inc., Toronto, Canada.

Temme, C., Blanchard, P., Steffen, A., Banic, C., Beauchamp, S., Poissant, L., Tordon, R., Wiens, B., 2007. Trend, seasonal and multivariate analysis study of total gaseous mercury data from the Canadian atmospheric mercury measurement network (CAMNet). Atmos. Environ. 41 (26), 5423–5441.

Theil, H., 1950. A rank-invariant method of linear and polynomial regression analysis. Indag. Math. (N.S.) 12 (85), 173.

Tørseth, K., Aas, W., Breivik, K., Fjæraa, A., Fiebig, M., Hjellbrekke, A., Myhre, C.L., Solberg, S., Yttri, K., 2012. Introduction to the European monitoring and evaluation programme (EMEP) and observed atmospheric composition change during 1972–2009. Atmos. Chem. Phys. 12 (12), 5447–5481. http://dx.doi.org/10.5194/acp-12-5447-2012.

Travnikov, O., Angot, H., Artaxo, P., Bencardino, M., Bieser, J., d'Amore, F., Dastoor, A., De Simone, F., Diéguez, M.d.C., Dommergue, A., et al., 2017. Multi-model study of mercury dispersion in the atmosphere: atmospheric processes and model evaluation. Atmos. Chem. Phys. 17 (8), 5271–5295.

Vardè, M., Barbante, C., Barbaro, E., Becherini, F., Bonasoni, P., Busetto, M., Calzolari, F., Cozzi, G., Cristofanelli, P., Dallo, F., et al., 2022. Characterization of atmospheric total gaseous mercury at a remote high-elevation site (Col Margherita Observatory, 2543 m asl) in the Italian Alps. Atmos. Environ. 271, 118917.

Veselik, P., Dvorska, A., Michalek, J., 2017. Half a year of co-located gaseous elemental mercury measurements: investigation of temporal changes in measurement differences. Fresenius Environ. Bull. 26 (5), 3128–3137.

Wang, S., McNamara, S.M., Moore, C.W., Obrist, D., Steffen, A., Shepson, P.B., Staebler, R.M., Raso, A.R., Pratt, K.A., 2019. Direct detection of atmospheric atomic bromine leading to mercury and ozone depletion. Proc. Natl. Acad. Sci. 116 (29), 14479–14484.

Weigelt, A., Ebinghaus, R., Manning, A., Derwent, R., Simmonds, P., Spain, T., Jennings, S., Slemr, F., 2015. Analysis and interpretation of 18 years of mercury observations since 1996 at Mace Head, Ireland. Atmos. Environ. 100 (1), 85–93. http://dx.doi.org/10.1016/j.atmosenv.2014.10.050.

Weiss-Penzias, P.S., Gay, D.A., Brigham, M.E., Parsons, M.T., Gustin, M.S., Ter Schure, A., 2016. Trends in mercury wet deposition and mercury air concentrations across the US and Canada. Sci. Total Environ. 568, 546–556.

Xing, H., Jin, S., 2023. Structure and variations of global planetary boundary layer top from 2008–2022 multiple GNSS RO observations. J. Atmos. Sol.-Terr. Phys. 252, 106155.

Yue, F., Angot, H., Blomquist, B., Schmale, J., Hoppe, C.J., Lei, R., Shupe, M.D., Zhan, L., Ren, J., Liu, H., et al., 2023. The Marginal Ice Zone as a dominant source region of atmospheric mercury during central Arctic summertime. Nature Commun. 14 (1), 4887.

Zhang, H., Fu, X., Lin, C.J., Shang, L., Zhang, Y., Feng, X., Lin, C., 2016a. Monsoon-facilitated characteristics and transport of atmospheric mercury at a high-altitude background site in southwestern China. Atmos. Chem. Phys. 16 (20), 13131–13148.

Zhang, H., Fu, X., Yu, B., Li, B., Liu, P., Zhang, G., Zhang, L., Feng, X., 2021. Speciated atmospheric mercury at the Waliguan Global Atmosphere Watch station in the northeastern Tibetan Plateau: implication of dust-related sources for particulate bound mercury. Atmos. Chem. Phys. 21 (20), 15847–15859.

Zhang, Y., Jacob, D.J., Horowitz, H.M., Chen, L., Amos, H.M., Krabbenhoft, D.P., Slemr, F., St. Louis, V.L., Sunderland, E.M., 2016b. Observed decrease in atmospheric mercury explained by global decline in anthropogenic emissions. Proc. Natl. Acad. Sci. 113 (3), 526–531.

Zhang, Y., Zhang, P., Song, Z., Huang, S., Yuan, T., Wu, P., Shah, V., Liu, M., Chen, L., Wang, X., et al., 2023. An updated global mercury budget from a coupled atmosphere-land-ocean model: 40% more re-emissions buffer the effect of primary emission reductions. One Earth 6 (3), 316–325.

Zimmermann, P., Feichter, J., Rath, H., Crutzen, P., Weiss, W., 1989. A global three-dimensional source-receptor model investigation using 85Kr. Atmos. Environ. (1967) 23 (1), 25–35.